

# Strengthening Generative Robot Policies through Predictive World Modeling

Han Qi<sup>\*1</sup>, Haocheng Yin<sup>\*1</sup>, Yilun Du<sup>1</sup>, Heng Yang<sup>1</sup>

<sup>1</sup>School of Engineering and Applied Sciences, Harvard University

<https://computationalrobotics.seas.harvard.edu/GPC>

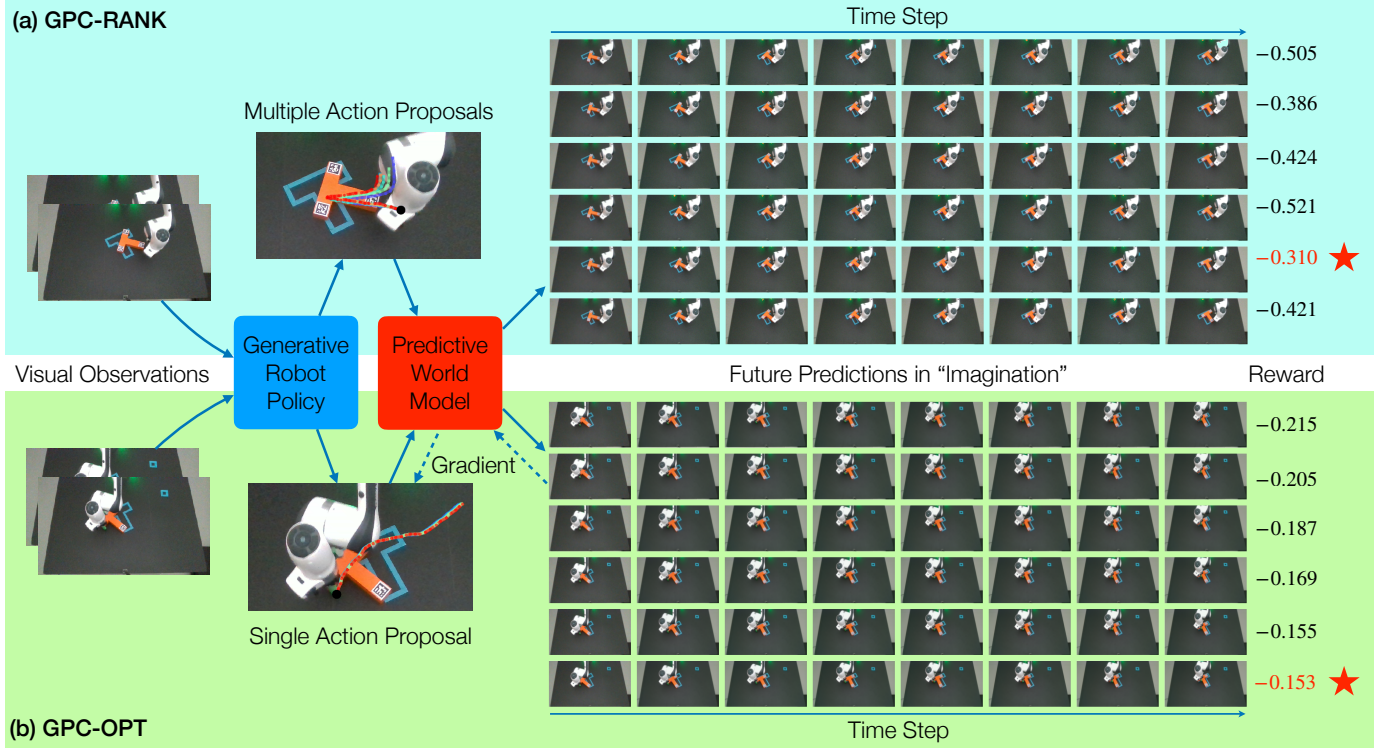


Fig. 1: GENERATIVE PREDICTIVE CONTROL (GPC). Given visual (or state) observations, a generative policy—trained from behavior cloning—proposes an action chunk. Conditioned on the action chunk and past observations, a predictive world model—trained from diverse trajectories—predicts the future observations in “imagination”. In (a) GPC-RANK, the policy outputs multiple action proposals and for each proposal the world model predicts its future and associated reward. The proposal with highest reward is executed. In (b) GPC-OPT, the policy outputs a single action proposal and multiple gradient ascent steps are performed to optimize the action proposal for higher reward. Both GPC-RANK and GPC-OPT dominate pure behavior cloning.

**Abstract**—We present generative predictive control (GPC), a learning control framework that (i) clones a *generative diffusion-based policy* from expert demonstrations, (ii) trains a *predictive action-conditioned world model* from both expert demonstrations and random explorations, and (iii) synthesizes an online planner that ranks and optimizes the action proposals from (i) by looking ahead into the future using the world model from (ii). Crucially, we show that *conditional video diffusion* allows learning (near) physics-accurate *visual world models* and enable robust visual foresight. Focusing on planar pushing with rich contact and collision, we show GPC dominates behavior cloning across state-based and vision-based, simulated and real-world experiments.

## I. INTRODUCTION

State-of-the-art robot control policies are synthesized using two major paradigms:

- **Predictive control.** With access to a predictive dynamical model of the robot and its physical environment, *optimal control* (OC) and (deep) *reinforcement learning* (RL) are the workhorses for designing performant controllers in locomotion [57], manipulation [4], and aviation [1, 31]. While OC typically designs controllers based on analytic dynamical models and online optimization [30], RL can learn a policy via interactions with a complicated and black-box dynamical model [49], either through simulation or in the real world. The nature of predictive control is to *look ahead*, by anticipating how the environment

<sup>\*</sup>Equal contribution

will change and how much reward will be collected.

- **Generative control.** Motivated by the success of generative modeling in vision and language, generative control—learning a controller from expert demonstrations using *behavior cloning* with generative models—is rapidly rising to prominence [15, 52]. Due to the abundance of demonstrations and the unprecedented distribution learning capacity of generative models, generative control has led to *robot foundation policies* capable of solving diverse tasks from vision and language [21]. The nature of generative control is to *look back*, making decisions based on expert policies in the past.

Each paradigm has its advantages and limitations. When dynamics modeling is accurate and tractable, predictive control delivers precision and robustness (e.g., Boston Dynamics parkour and SpaceX rocket landing). However, in many cases (e.g., manipulation with contact [35] and deformable objects [65], vision-based control [48]), the dynamics can be inaccurate or computationally expensive for optimization (as in OC) and interaction (as in RL). Generative control, on the other hand, circumvents the need for careful dynamics modeling and directly learns the policy via generative modeling of the expert demonstrations. However, generative control suffers from distribution shifts (due to its supervised learning nature [38, 21]) and lack of precision and robustness (i.e., they can do lots of tasks but do few of them as well as specialized controllers [19, 10]). Moreover, whether the “scaling law” can address these issues is questionable [7, 63, 62].

Humans, nevertheless, look back *and* look ahead when making decisions. We look back at similar past experiences to shortlist a set of proper actions, and look ahead—unroll the environment dynamics in “imagination”—to predict which action plan is optimal in terms of certain metrics.

*Can we establish a similar robot control paradigm that both looks back (i.e., generative) and looks ahead (i.e., predictive)?*

**Contribution.** We propose *generative predictive control* (GPC), a framework that combines a generative robot policy with a predictive dynamical model of the world (i.e., a world model [22]). GPC contains three modules (*cf.* Fig. 1):

- **Generative policy training.** Given expert demonstrations, GPC uses generative modeling to train a policy that approximates the conditional distribution of expert “*action chunks*” given past observations.
- **Predictive world modeling.** A world model simulates future observations conditioned on action chunks and past observations. One would naturally want to learn the world model using the same expert demonstrations as in policy training. However, such a world model can only simulate dynamics of the expert policy and thus is not effective for correcting policy error (see §IV). We show that adding “*random exploration*” data—cheaper to collect—enriches the data distribution and yield a world model that strengthens the policy at test time. For state-based world modeling, a simple MLP is sufficient to learn accurate dynamics. For vision-based world modeling, we

capitalize on *conditional video diffusion* [25, 6] to predict action-conditioned future observations.

- **Online planning.** Inspired by classical model predictive control, and assuming a reward model is available, GPC uses two lightweight online algorithms to strengthen the generative policy with the predictive world model. The first one, GPC-RANK, samples many action proposals from the policy, unrolls the future conditioned on each proposal, and selects the proposal with highest reward. The second one, GPC-OPT, treats the action proposal from the policy as a “warmstart” and optimizes it to maximize reward using gradient ascent, a technique known as *single shooting* [16]. These two algorithms can be easily combined to perform gradient-based optimization on multiple action proposals (warmstarts) and select the best one.

We evaluate GPC in both simulated and real-world, state-based and vision-based robotic manipulation tasks, demonstrating significant improvement over pure behavior cloning.

**Novelty.** Among the three modules of GPC, the first one is not new and has become the common practice in robot policy learning [15, 52]. The novelty of GPC lies in learning a predictive world model—crucially, using random exploration data—to strengthen the generative policy with *online planning* (as opposed to, e.g., offline RL [23, 28, 56, 17, 44]). Moreover, different from previous works leveraging generative models for world modeling, GPC learns a world model that is explicitly *action-conditioned*. In other words, the world model is “controllable” by the robot’s actions. We show such a controllable world model enables robust real-world robotic manipulation.

**Paper organization.** We formalize the overall pipeline of GPC in §II and detail the approaches for state-based and vision-based world modeling in §III. We present experimental results in §IV and conclude in §VI. Review of related works and how GPC differs from them are described in §V.

## II. OVERVIEW OF GENERATIVE PREDICTIVE CONTROL

Let  $I_t$  be the information vector summarizing the state of the robot and the environment up to time step  $t$ . For state-based robot control,  $I_t := x_t$  is the (low-dimensional) state of the robot and its environment (e.g., poses); for vision-based robot control,  $I_t := o_{t-H:t}$  is the history of (high-dimensional) visual observations where each  $o_t$  is a single (or multi-view) image(s). Let  $a_t$  be the robot action at time  $t$  and  $a_{t:t+T}$  be an *action chunk* of length  $T+1$ . Our goal is to design a robot control policy that decides  $a_{t:t+T}$  based on  $I_t$  to solve certain tasks (e.g., described by language instructions).

Let us formalize the three modules of GPC.

**Generative policy training.** We ask humans to teleoperate robots to solve the tasks. The expert demonstrations are then divided into clips of data containing pairs of state information and action chunks, i.e., a dataset  $\mathcal{D}_{\text{expert}}^P = \{I_t^i \leftrightarrow a_{t:t+T}^i\}_{i=1}^{N_{\text{expert}}}$  with number of samples  $N_{\text{expert}}$ . Policy learning becomes a supervised learning problem with input  $I_t$  and output  $a_{t:t+T}$ .<sup>1</sup> In

<sup>1</sup> It is also common to include language instructions as input to the policy as in vision-language-action (VLA) models [32]. GPC can generalize to VLAs in a straightforward way. We exclude language here to focus on motion planning.

GPC, we follow the diffusion policy learning framework [15]. Specifically, we feed  $I_t$  into a network that parametrizes the score function of the conditional distribution  $p(a_{t:t+T}|I_t)$ , using which Gaussian noise vectors are gradually diffused to expert action chunks. The score function network is trained using denoising prediction [24]. Policy learning leads to a policy network  $\mathcal{P}(\cdot)$  that predicts action chunks  $a_{t:t+T}$  given state information  $I_t$ . It is important to note that  $\mathcal{P}(\cdot)$  is *stochastic* and effectively a sampler from the (approximate) conditional distribution  $p(a_{t:t+T}|I_t)$ , meaning that given  $I_t$ , we can draw many possible action chunks  $(a_{t:t+T}^{(1)}, \dots, a_{t:t+T}^{(K)})$  from  $\mathcal{P}(\cdot)$ . We call each action chunk  $a_{t:t+T}$  an *action proposal*.

**Predictive world modeling.** The fact that  $\mathcal{P}(\cdot)$  is stochastic leads to a natural question: which one of the  $K$  action proposals should be selected? The world model precisely aims to answer this question by predicting the future consequences of each action proposal. To build the world model, we need pairs of  $(I_t, a_{t:t+T})$  (current state information plus an action chunk) and  $I_{t+1:t+T+1}$  (future state information). The expert demonstrations used for policy training already contain such pairs, i.e., a dataset  $\mathcal{D}_{\text{expert}}^W = \{(I_t^i, a_{t:t+T}^i) \leftrightarrow I_{t+1:t+T+1}^i\}_{i=1}^{N_{\text{expert}}}$ . Nevertheless, as we show in §IV, if we train the world model only using  $\mathcal{D}_{\text{expert}}^W$ , the predictive power of the world model is insufficient to guide action proposal selection. One can collect more expert demonstrations to enlarge the datasets, but it can be expensive. Instead, we posit that *random exploration* data are not only easier to collect, but also rich in dynamics. Therefore, we collect another exploration dataset  $\mathcal{D}_{\text{explore}}^W = \{(I_t^i, a_{t:t+T}^i) \leftrightarrow I_{t+1:t+T+1}^i\}_{i=1}^{N_{\text{explore}}}$  where humans (or any other controllers) are asked to randomly perturb the system without solving any tasks. In control theory terminology, the goal of this is to perform “system identification” with “sufficient excitation” [37]. We combine the two datasets  $\mathcal{D}^W := \mathcal{D}_{\text{expert}}^W \cup \mathcal{D}_{\text{explore}}^W$  to train the world model. Details of the design of the world model architecture are deferred to §III. For now, the reader can assume we obtain a model  $\mathcal{W}(\cdot)$  that predicts the future  $I_{t+1:t+T+1}$  conditioned on the current state information and the action proposal  $(I_t, a_{t:t+T})$ .

**Online planning.** We now formalize the two online planning algorithms, namely GPC-RANK and GPC-OPT, that combine the policy  $\mathcal{P}(\cdot)$  and the world model  $\mathcal{W}(\cdot)$  (cf. Fig. 1). We assume a reward model  $\mathcal{R}(\cdot) : I_{t+1:t+T+1} \rightarrow r_t$  is available that predicts the reward given the future state information, e.g., a small neural network that is separately trained.

(i) GPC-RANK is based on the simple intuition to pick the action proposal with highest reward. Formally, we sample  $K$  action proposals from the policy

$$(a_{t:t+T}^{(1)}, \dots, a_{t:t+T}^{(k)}, \dots, a_{t:t+T}^{(K)}) \sim \mathcal{P}(I_t), \quad (1)$$

and output the best proposal by passing them through the world model  $\mathcal{W}(\cdot)$  and computing respective rewards:

$$\pi(I_t) = a_{t:t+T}^{(k_\star)}, \quad k_\star \in \arg \max_{k=1, \dots, K} \mathcal{R}(\mathcal{W}(I_t, a_{t:t+T}^{(k)})), \quad (2)$$

where we used the notation  $\pi(\cdot)$  to denote the online policy in contrast to the offline policy  $\mathcal{P}(\cdot)$ . The underly-

ing assumption of GPC-RANK is that, due to distribution shifts, the optimal action chunk at test time may not have the highest likelihood in  $\mathcal{P}(\cdot)$ , and thus may need more samples to be discovered. The world model—assuming it is learned from a richer distribution because of random exploration—will pick up the optimal action chunk through (2). A nice property of GPC-RANK is that it can be easily parallelized.

(ii) GPC-OPT takes a different perspective by directly solving the reward maximization problem given the world model:

$$\max_{a_{t:t+T}} \mathcal{R}(\mathcal{W}(I_t, a_{t:t+T})), \quad (3)$$

where the action chunk are viewed as decision variables. The difficulty is, however, problem (3) can be highly nonconvex due to the nonlinearity and nonsmoothness of  $\mathcal{W}(\cdot)$  and  $\mathcal{R}(\cdot)$ . Fortunately, the pretrained policy  $\mathcal{P}(\cdot)$  comes to rescue because it narrows down the search space by providing good initializations to solve (3), i.e., warmstarts. Formally, we sample an action chunk  $\hat{a}_{t:t+T}$  from  $\mathcal{P}(\cdot)$  and perform  $M$  steps of gradient ascent starting from  $\hat{a}_{t:t+T}$  (assuming  $\mathcal{R}(\cdot)$  is differentiable):

$$\begin{aligned} \hat{a}_{t:t+T}^{(0)} &:= \hat{a}_{t:t+T} \sim \mathcal{P}(I_t), \text{ and for } \ell = 1, \dots, M \text{ do:} \\ \hat{a}_{t:t+T}^{(\ell)} &= \hat{a}_{t:t+T}^{(\ell-1)} + \eta^{(\ell)} \nabla_{a_{t:t+T}} \mathcal{R}(\mathcal{W}(I_t, \hat{a}_{t:t+T}^{(\ell-1)})), \end{aligned} \quad (4)$$

where  $\eta^{(\ell)} > 0$  are step sizes. The online policy outputs the final optimized action chunk

$$\pi(I_t) = \hat{a}_{t:t+T}^{(M)}. \quad (5)$$

Since the gradients in (4) are readily available from automatic differentiation, gradient ascent can be carried out using off-the-shelf optimizers like ADAM. Readers familiar with the optimal control literature will recognize GPC-OPT is the classical single shooting algorithm [16]. Compared to GPC-RANK which evaluates the world model  $K$  times, GPC-OPT evaluates the world model  $M$  times. The former can be parallelized but the latter cannot.

GPC-RANK and GPC-OPT can be combined. We can sample  $K$  action proposals from  $\mathcal{P}(\cdot)$  and for each proposal perform reward maximization according to (4), leading to  $K$  optimized action chunks. We pick the optimized action chunk with highest reward. GPC-RANK+OPT can be viewed as solving the optimization (3) from multiple initializations [50], and requires  $K \times M$  evaluations of the world model.

We provide a succinct summary of GPC in Algorithm 1.

**Remark 1** (Connection with Offline RL). *It is worth noting that the composition of the reward model  $\mathcal{R}(\cdot)$  and the world model  $\mathcal{W}(\cdot)$  can be identified as the so-called Q-value function in offline RL, as they predict the reward of an action chunk  $a_{t:t+T}$  given the current information  $I_t$ . However, there are three subtle differences between GPC and offline RL. (a) GPC learns an explicit dynamics model instead of just approximating the Q-value function (this is similar to model-based offline RL). (b) The composition of  $\mathcal{R}(\cdot)$  and  $\mathcal{W}(\cdot)$  provides a Q-value function for “action chunks” while the usual Q-value*

**Algorithm 1:** Generative Predictive Control (GPC)

---

**Input:** Expert action demonstrations  
 $\mathcal{D}_{\text{expert}}^P = \{I_t^i \leftrightarrow a_{t:t+T}^i\}_{i=1}^{N_{\text{expert}}}$ ; Expert  
 trajectories and random exploration trajectories  
 $\mathcal{D}_{\text{expert}}^W \cup \mathcal{D}_{\text{explore}}^W = \{(I_t^i, a_{t:t+T}^i) \leftrightarrow$   
 $I_{t+1:t+T+1}^i\}_{i=1}^{N_{\text{expert}}+N_{\text{explore}}}$ ; Reward model  $\mathcal{R}$ ;  
 Positive integers  $K, M$

1 // Generative policy training  
 2  $\mathcal{P}(\cdot) \leftarrow \text{BEHAVIORCLONING}(\mathcal{D}_{N_{\text{expert}}}^P)$ ;  
 3 // Predictive world modeling (§III)  
 4  $\mathcal{W}(\cdot) \leftarrow \text{DYNAMICSLEARNING}(\mathcal{D}_{\text{expert}}^W \cup \mathcal{D}_{\text{explore}}^W)$ ;  
 5 // Online planning given  $I_t$   
 6 **for**  $k = 1, \dots, K$  **do**  
 7   // Sample action proposal  
 8    $a_{t:t+T}^{(k)} \sim \mathcal{P}(I_t)$ ;  
 9   // Maximize reward  
 10   Set  $\hat{a}_{t:t+T}^{(0)} = a_{t:t+T}^{(k)}$ ;  
 11   **for**  $\ell = 1, \dots, M$  **do**  
 12      $\hat{a}_{t:t+T}^{(\ell)} = \hat{a}_{t:t+T}^{(\ell-1)} + \eta^{(\ell)} \nabla_{a_{t:t+T}} \mathcal{R}(\mathcal{W}(I_t, \hat{a}_{t:t+T}^{(\ell-1)}))$ ;  
 13     Set  $a_{t:t+T}^{(k)} = \hat{a}_{t:t+T}^{(M)}$ ;  
 14 // Rank optimized action proposals  
 15 Find  $k_* \in \arg \max_{k=1, \dots, K} \mathcal{R}(\mathcal{W}(I_t, a_{t:t+T}^{(k)}))$ ;  
 16 Return  $a_{t:t+T}^{(k_*)}$ ;

---

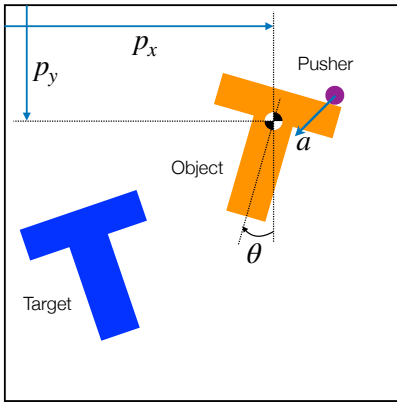


Fig. 2: ILLUSTRATION OF PLANAR PUSHING.

function involves a single action. (c) GPC learns the dynamics model using diverse trajectories (without rewards), instead of only expert demonstrations. In §IV, we compare GPC with an offline RL method adapted from single action to action chunk and show that GPC outperforms offline RL.

The above overview of GPC highlights the importance of the world model in both ranking and optimizing action proposals. Indeed, the concept of a learned world model dates back to early pioneering works on deep visual foresight [20]. In the next section, we will show that modern diffusion models are the key enabler for learning (near) physics-accurate visual world models that were not possible before.

### III. WORLD MODEL LEARNING

Recall that the world model takes as input  $(I_t, a_{t:t+T})$  and outputs  $I_{t+1:t+T+1}$ . We will briefly present the world model design when  $I_t = x_t$  contains low-dimensional states (§III-A) and focus on a diffusion-based world model when  $I_t = o_{t-H:t}$  contains high-dimensional images (§III-B).

**Planar pushing.** Before getting started, since we will focus on planar pushing in our experiments §IV, we briefly introduce the problem setup. As shown in Fig. 2, the planar pushing task involves pushing an object (e.g., a T block) to align with the target using a pusher. We assume the target position is fixed and known, and hence we do not need to predict it. The state of the object is fully described by its 2D coordinates  $p = (p_x, p_y)$  and 1D angle  $\theta$ . The action space is  $a \in \mathbb{R}^2$  containing pushing velocities in the  $x$  and  $y$  directions. We choose the planar pushing task for two reasons. First, it is easy to understand and simple to visualize. Second, it is also a long-standing difficult task because it is *contact-rich*. Depending on whether the pusher makes or breaks contact and whether the contact is sticking or sliding, the dynamics of the task involves multiple different modes and requires intricate physics reasoning [26]. This makes planar pushing a both elementary and challenging task for world model learning.

#### A. State-based World Modeling

For state-based world modeling, with  $x = (p, \theta)$  being the state of the object, we learn a single-step dynamics model:

$$x_{t+1} = f_{\text{state}}(x_t, a_t). \quad (6)$$

As pointed out by [64], when rotations are involved in machine learning, it is crucial to choose a rotation representation that is continuous. For example, the angle representation  $\theta$  is discontinuous due to the “wrap  $2\pi$ ” issue. Therefore, we augment the state as

$$x = (p, \cos(\theta), \sin(\theta)) \quad (7)$$

for both the input and output of  $f_{\text{state}}$  in (6) (we normalize the output of  $f_{\text{state}}$  to satisfy  $\sin^2(\cdot) + \cos^2(\cdot) = 1$ ). We also found it beneficial to have two separate networks, one predicting the position and the other predicting the rotation. In our implementation, for each of the network, we used a six-layer MLP with hidden dimension 128.

During testing, we need to predict  $T$  steps into the future given a sequence of actions  $a_{t:t+T}$ . We do so by recursively applying the single-step predictor (6). As we will show in §IV, this simple MLP-based single-step predictor is sufficient for robust online planning.

#### B. Vision-based World Modeling

State-based world modeling requires accurate state estimation, which is possible in a lab environment with infrastructure such as AprilTags [46] or motion capture but can be challenging in the open environment. Therefore, it is desired to directly learn *visual dynamics*, i.e., a visual world model.

**Diffusion-based visual world modeling.** Motivated by the success of using diffusion models for image generation, we

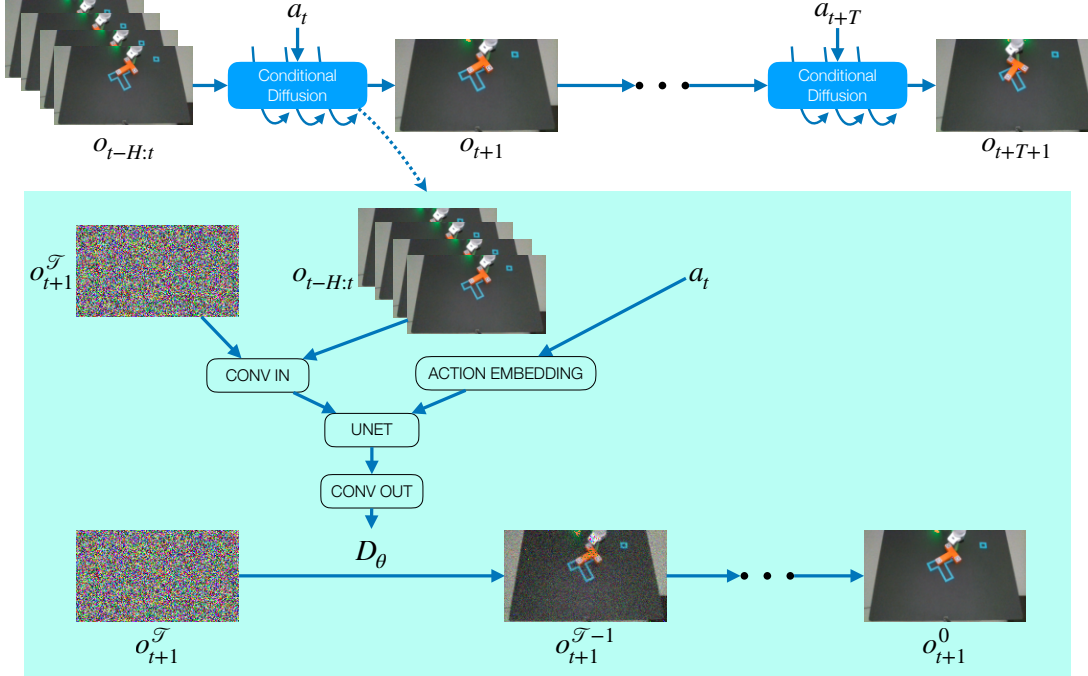


Fig. 3: DIFFUSION-BASED VISUAL WORLD MODELING. Our visual world model consists of a sequence of recursive single-step image predictors. Each single-step image predictor is designed as a conditional diffusion process.

design a visual world model based on conditional diffusion. Recall that the input to the world model is  $I_t = o_{t-H:t}$  (the sequence of past images) and  $a_{t:t+T}$ , and the output is  $I_{t+1:t+T+1} := o_{t+1:t+T+1}$  (a sequence of future images). Similar as the state-based world modeling, we design the visual world model as a recursive application of single-step image predictors. We denote the single-step predictor as

$$o_{t+1} = f_{\text{vision}}(o_{t-H:t}, a_t), \quad (8)$$

where  $f_{\text{vision}}$  is a conditional diffusion model. The unique property of diffusion is that  $o_{t+1}$  is not generated in a single feedforward step, but rather through a sequence of denoising steps. In particular, let  $o_{t+1}^{\mathcal{T}}$  be drawn from a white Gaussian noise distribution, then  $f_{\text{vision}}$  proceeds as:

$$o_{t+1}^{\mathcal{T}-1} = D_{\phi}(o_{t+1}^{\mathcal{T}}, \tau, o_{t-H:t}, a_t), \tau = \mathcal{T}, \dots, 1, \quad (9)$$

where  $\mathcal{T}$  is the total number of denoising steps and the output of  $f_{\text{vision}}$  is  $o_{t+1} = o_{t+1}^0$ . In (9),  $\tau$  is the denoising step index and  $D_{\phi}$ —the “denoiser”—is a neural network with weights  $\phi$ . We use the same architecture for  $D_{\phi}$  as in [5], which contains convolutions, action embedding, and a U-Net, as illustrated in Fig. 3. The denoiser  $D_{\phi}$  is trained by adding random noises to the clean images and then predicting the noise.

**Two-phase training.** To improve the accuracy and consistency of visual world modeling, we train it in two phases. In phase one, we train only the single-step image predictor (8), i.e., with supervision only on a single image  $o_{t+1}$ . In phase two, we recursively apply the single-step predictor (8) for  $T$  times to obtain a sequence of future images  $o_{t+1:t+T+1}$ , and jointly supervise them with groundtruth images.

We use observation horizon  $H = 4$  in the visual world modeling, and  $\mathcal{T} = 3$  diffusion steps in  $f_{\text{vision}}$ .

**Remark 2 (Freeze the Noise).** *It should be emphasized that the single-step image predictor  $f_{\text{vision}}$  in (8) is “stochastic” where the stochasticity comes from the randomness in the initial noise  $o_{t+1}^{\mathcal{T}}$ . In classical generative modeling, stochasticity is desired because we want the model to generate diverse images. However in our paper, we want to use the diffusion-based world model for control. That is, we want to understand the impact of the “action” on the future, rather than the impact of the random “noise” on the future. Therefore, we freeze the noise  $o_{t+1}^{\mathcal{T}}$  to be zero at inference time, which makes the world model deterministic—outputting the most likely future predictions (because  $o_{t+1}^{\mathcal{T}} = 0$  attains the peak probability in the Gaussian distribution). In fact, without freezing the noise, GPC-OPT does not work because the gradient of the reward with respect to the actions (cf. (4)) would be “contaminated” by the noise and thus does not guide online planning.*

#### IV. EXPERIMENTS

In this section, we focus on evaluation of the GPC framework on planar pushing and comparison to baseline behavior cloning. As mentioned in §III, we choose planar pushing because it is an elementary but also quite challenging task due to the complicated contact and collision dynamics involved.

##### A. State-based Planar Pushing in Simulation

We first study the setup where the groundtruth state of the object (i.e.,  $(p_x, p_y, \theta)$ ) is available through a simulator. We use the same simulator as in [15] with a T-shape object.

**Policy.** We first train a state-based diffusion policy  $\mathcal{P}(\cdot)$  [15] from which we can draw *action proposals*, as explained in §II. We use 500 expert demonstrations to train the policy network for 300 epochs with AdamW optimizer of learning rate  $10^{-4}$

and weight decay  $10^{-6}$ . We use observation horizon  $H = 2$ , prediction horizon  $T = 16$ , and action horizon 8.<sup>2</sup>

**World model.** Then we need the world model to predict the future consequences of each action proposal. As in §III-A, we use MLP networks to build a single-step state predictor and recursively apply it  $T$  times to form the world model  $\mathcal{W}(\cdot)$ . As introduced in §II, to ensure the dynamics of the world model is learned from a richer distribution than the expert demonstrations, the training dataset of the world model is expanded with random exploration demonstrations which attempt to record more pusher-object interactions at different contact points. To be specific, we let human operators (who are different from the operator of the expert demonstrations) collect 7 long random play demonstrations and 1 special long demonstration that randomly collides the object with the boundary wall. In addition, we also generate 7 sets of “noisy expert demonstrations” where the original expert actions are contaminated with different scales of Gaussian noise.

**Reward.** After obtaining the predicted consequences of the action proposals (i.e., predicted future states of  $p_x, p_y, \theta$  of the object), we define the reward  $\mathcal{R}(\cdot)$  using a *registration loss* between the target and the object. Particularly, the registration loss computes the sum of the squared distances between the vertices of the object and the target. Clearly, this reward function is differentiable with respect to the predicted states.

**Online planning.** Now we can use the policy  $\mathcal{P}(\cdot)$ , the world model  $\mathcal{W}(\cdot)$ , and the reward model  $\mathcal{R}(\cdot)$  for online planning, as prescribed in the GPC Algorithm 1. Specifically, In GPC-RANK, we pick the action chunk with highest reward (smallest registration loss) from the  $K$  action proposals. In GPC-OPT, we sample one action chunk from  $\mathcal{P}(\cdot)$  and perform  $M$  steps of gradient ascent to optimize this action chunk for a higher reward (smaller registration loss). In GPC-RANK+OPT, we sample  $K$  action proposals, perform  $M$  gradient ascent steps for each of the action proposal, and finally pick the *optimized* action chunk with the highest reward.

**Questions.** We hope to answer the following questions through our experiments:

- How much does GPC outperform the state-of-art behavior cloning method (e.g., diffusion policy) and how do  $K$  and  $M$  affect the performance?
- How does GPC compare with Offline RL based method?
- What is the effect of training the world model using both expert and random exploration data?

**Results.** In Table I, we study how different variations of  $K$  and  $M$  affect the performance. When  $K = 1$  and  $M = 0$ , this is the baseline state-based diffusion policy trained from behavior cloning [15]. In GPC-RANK, if we increase the number of action proposals to  $K = 100$ , the score increases to around 0.9, which is about 10% increase from the baseline. Notably, due to parallelization inside GPC-RANK, the runtime does not increase when  $K = 100$ . We also tried larger  $K$ , such as 1000

<sup>2</sup>This means the policy is executed in a receding horizon fashion. The policy predicts 16 steps of future actions and only 8 of them are executed in the environment, which creates implicit feedback.

and 5000, and the performance further increases to 0.934. Note that in the last column of Table I, we provided a “performance upper bound” which is obtained by using the groundtruth simulator (instead of the learned world model) to rank action proposals at  $K = 5000$ . For GPC-OPT, if we sample one action proposal and perform gradient ascent from it (e.g., doing 30 gradient steps), the score can be increased to 0.886, which is also quite significant compared to the baseline. Then in GPC-RANK+OPT, we tried different combinations of  $K$  and  $M$ . The improvement remains substantial, indicating the robustness of GPC and shows both sampling multiple proposals and gradient-based optimization consistently improve the performance.

In the first two columns of Table I, we present the results for another baseline of using Offline RL to rank and select actions. The Offline RL method follows that of [44] and is described in Appendix A. Crucially, the Offline RL method only uses the expert demonstrations and does not leverage the random exploration data (because the random exploration data do not have labeled rewards). We can see that the performance of Offline RL is similar or even worse than the case of behavior cloning. A plausible reason for this is that the Offline RL method does not explicitly seek to learn the dynamics from the random explorations and hence the learned value function may be misleading for ranking action proposals.

Finally, in Table II, we present the results of using a world model trained without random exploration data. We observe that, when the world model is only trained from expert demonstrations, the performance of both GPC-RANK and GPC-OPT gets worse. This demonstrates the importance of using random exploration data to learn an accurate world model.

### B. Vision-based Planar Pushing in Simulation

We then proceed to vision-based planar pushing with the same T-shape object.

**Policy.** We train a vision-based diffusion policy  $\mathcal{P}(\cdot)$  [15] using ResNet18 as the vision encoder and UNet as the action diffusion network. We used 500 expert demonstrations to train the policy for 300 epochs with AdamW optimizer of learning rate  $10^{-4}$  and weight decay  $10^{-6}$ . We use observation horizon of 2, prediction horizon of 16, and action horizon of 9.

**World model.** As in §III-B, we use a diffusion model to build a single-step image predictor and recursively apply it  $T$  times to form the world model  $\mathcal{W}(\cdot)$ . Same as in §IV-A, the training data includes random explorations.

**Reward.** Different from the state-based planar pushing, since the future predictions are images, we cannot directly compute a reward signal. Therefore, we first train a pose prediction network with ResNet18 plus MLP, and then compute the registration loss using the predicted object pose. Note that this learned reward model  $\mathcal{R}(\cdot)$  is still differentiable.

**Online planning:** With the vision-based policy, the visual world model, and the learned reward model, we follow the same online planning protocol described in §IV-A.

**Quality of visual world modeling.** Before presenting the results of GPC for online planning, we first study whether our visual world modeling technique is better than some

	Offline RL		GPC-RANK				GPC-OPT	GPC-RANK+OPT			With GT simulator
	$K = 100$	$K = 5000$	$K=1$ $M=0$	$K=100$ $M=0$	$K=1000$ $M=0$	$K=5000$ $M=0$	$K=1$ $M=30$	$K=10$ $M=30$	$K=20$ $M=30$	$K=30$ $M=20$	
Score	0.788	0.745	0.812	0.898	0.932	0.934	0.886	0.912	0.914	0.891	0.952

TABLE I: STATE-BASED PLANAR PUSHING (PUSH-T) IN SIMULATION. Score is measured by the IoU metric averaged over 100 evaluation seeds.  $K$  is the number of action proposals sampled from  $\mathcal{P}(\cdot)$  while  $M$  is the number of gradient steps performed to maximize reward.

	GPC-RANK				GPC-OPT
	$K = 100, M = 0$	$K = 1000, M = 0$	$K = 5000, M = 0$	$K = 1, M = 30$	
Score (using world model trained <i>without</i> random exploration)	0.832	0.838	0.816	0.752	
Score (using world model trained <i>with</i> random exploration)	0.898	0.932	0.934	0.886	

TABLE II: THE IMPORTANCE OF RANDOM EXPLORATION IN WORLD MODEL LEARNING (STATE-BASED PUSH-T).



Fig. 4: COMPARISON OF DIFFERENT VISUAL WORLD MODELING TECHNIQUES ON TWO EXAMPLES.

baselines. Particularly, we chose two baselines, one from the pioneering deep visual foresight [20], and the other from the more recent AVDC paper [19]. The world model in deep visual foresight leverages CNN and LSTM for future prediction, and we follow the Github implementation.<sup>3</sup> AVDC is originally designed for video diffusion conditioned on language, and we modify its official implementation<sup>4</sup> to condition on robot actions. Notably, AVDC is a multiple-step world model as it simultaneously diffuses future images together, unlike our recursive structure. Fig. 4 compares the quality of future predictions of three methods (ours, deep visual foresight, and AVDC) against the groundtruth in two examples. We see that diffusion-based visual world modeling (ours and AVDC) clearly dominates the classical deep visual foresight. Between ours and AVDC, we can observe that the future predictions from our method are better aligned with the groundtruth.

**Planning performance.** Same as §IV-A, we study the impact of  $K$  and  $M$  on the performance of GPC, its comparison with Offline RL, and the importance of random exploration.

In Table III, we study how different variations of  $K$  and  $M$  affect the performance of GPC. We can see that (a) GPC-RANK increases around 15% from the diffusion policy baseline (when  $K = 1, M = 0$ ); (b) GPC-OPT increases around 25% from the diffusion policy baseline; and (c) GPC-RANK+OPT increases up to 40% from the baseline. Contrasting the vision-based results with the state-based results, we observe that GPC-OPT

appears to have a larger advantage in vision-based push-T. This indeed makes sense because the baseline vision-based diffusion policy only has a score of 0.642, leaving a lot of room for optimization to find better actions.

In the first column of Table III, we show the results of Offline RL. Unfortunately, Offline RL still does not perform as well as even the baseline vision-based diffusion policy.

In Table IV, we compare the performance of GPC-RANK and GPC-OPT when trained with or without random exploration. Consistent with our observations in IV-A, without training on random exploration, the performance of online planning significantly decreases.

#### C. Real-world Vision-based Planar Pushing

We then test GPC in real-world planar pushing. We not only show GPC is effective in “plain push-T”, but also show it can work for push-T with collision objects.

**Setup.** Fig. 5 depicts our real-world setup for vision-based planar pushing. The pusher is attached to the end-effector of a Franka Panda robotic arm to push a T block into the target position. An overhead Intel RealSense camera is used to provide image observations to the pusher. To train the reward model, we need to obtain block information as training data so we attached three AprilTags [46] to the T-block, which enables accurate pose estimation from image frames even in the case of occlusion. To collect real-world expert demonstrations, we follow Chi et al. [15] and use a SpaceMouse to teleoperate the robotic arm to push the T block. A and R blocks are the objects that T may collide into during pushing.

<sup>3</sup>[https://github.com/Xiaohui9607/physical\\_interaction\\_video\\_prediction\\_pytorch](https://github.com/Xiaohui9607/physical_interaction_video_prediction_pytorch)

<sup>4</sup><https://github.com/flow-diffusion/AVDC>

	Offline RL	GPC-RANK				GPC-OPT	GPC-RANK+OPT	
	$K = 100$	$K = 1, M = 0$	$K = 50, M = 0$	$K = 100, M = 0$	$K = 200, M = 0$	$K = 1, M = 25$	$K = 5, M = 10$	$K = 10, M = 25$
Score	0.620	0.642	0.698	0.739	0.719	0.791	0.824	0.882

TABLE III: VISION-BASED PLANAR PUSHING (PUSH-T) IN SIMULATION. Score is measured by the IoU metric averaged over 100 evaluation seeds.  $K$  is the number of action proposals and  $M$  is the number of gradient steps.

	GPC-RANK	GPC-OPT
	$K = 100, M = 0$	$K = 1, M = 25$
Score (using world model trained <i>without</i> random exploration)	0.647	0.652
Score (using world model trained <i>with</i> random exploration)	0.739	0.791

TABLE IV: THE IMPORTANCE OF RANDOM EXPLORATION IN WORLD MODEL LEARNING (VISION-BASED PUSH-T).

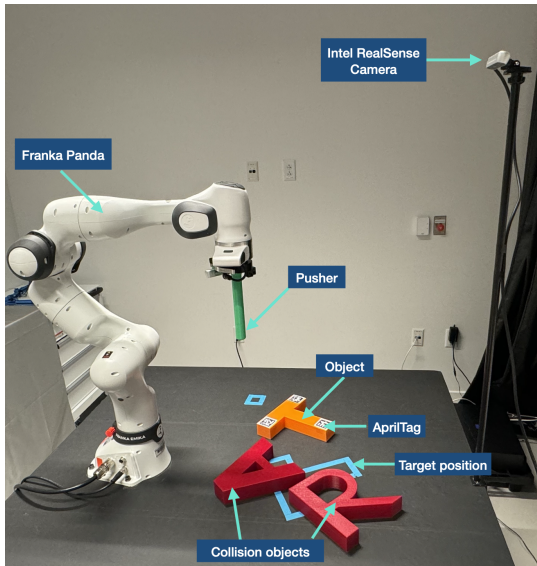


Fig. 5: REAL-WORLD SETUP.

1) *Plain push-T*: We first test on plain push-T (i.e., without collision with other objects). We train the policy with 100 expert push-T demonstrations using the architecture mentioned in §IV-B. Because of the slower moving speed of real-world pusher, we use a larger prediction horizon  $T = 32$ . Same as §IV-B, we train the world model using all expert demonstrations and a few random explorations. For the reward model, we rely on AprilTag [46] to obtain the ground-truth object poses and use them to train the reward model  $\mathcal{R}(\cdot)$ . To be clear, our GPC pipeline in real world is still purely vision-based and the AprilTags are only used to obtain training data for the reward model (training the pose predictor). We follow the same online planning protocol described in §IV-A. We test GPC-RANK and GPC-OPT on a set of 10 push-T tasks where the T block is initialized at positions not seen during training.

**Performance.** While the baseline model succeeds 5 out of 10 times, GPC-RANK succeeds 7 out of 10 times and GPC-OPT succeeds 7 out of 10 times. Fig. 10(a) shows the trajectories for one test. More testing trajectories are shown in Appendix B and supplementary videos.

**Quality of world model predictions.** Fig. 6 shows the quality of world model prediction of push T for GPC-RANK and GPC-OPT. The images shown are all **predicted** by the world

model. They not only have very good visual effect and look realistic, but also they can accurately predict the dynamics reaction from given actions. From the last column, we can see even when the differences between action sequences are very small, the world model can still capture the details and predict the reaction in a meticulous way. This is very important to make GPC work.

2) *Push-T under collision*: Next, we hope to investigate how GPC works under more complex scenarios, involving harder tasks and more complex dynamics. We put an object of shape “A” on top of the target position so that when pushing T, it will inevitably collide with object A. The training data is 100 push-T expert demos with collision of A and some random exploration demos.

**Performance.** We test 5 seeds in total, and baseline model, GPC-RANK, GPC-OPT succeed for 2, 4, 3 seeds respectively.

We then proceed to test in an even harder situation: we put objects of shape “A” and “R” on top of the target position at the same time. Case 1: When pushing T, T may collide with A and R at the same time. Case 2: When pushing T, T would collide with one letter (e.g., “R”) and this letter will collide with another letter (e.g., “A”). We train the policy and world model here using 100 plain push-T expert demonstrations, 100 push-T colliding A expert demonstrations, and 100 push-T colliding A&R expert demonstrations.

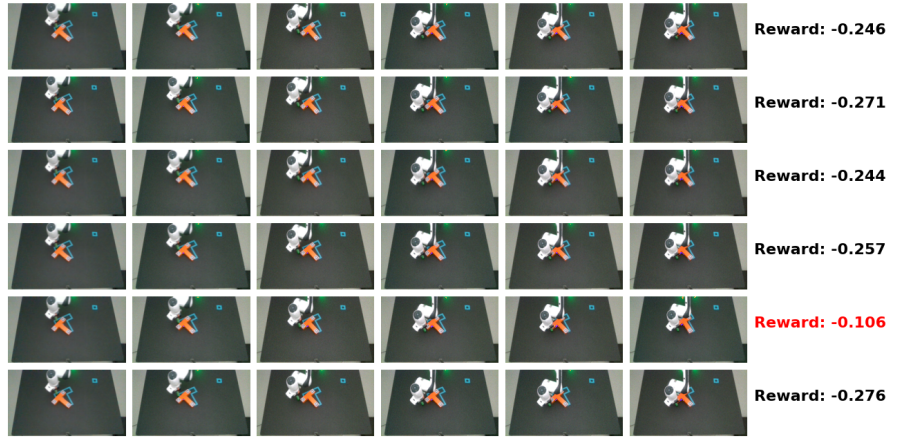
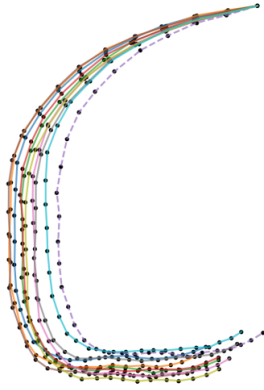
**Performance.** In the total of 5 testing seeds, baseline model, GPC-RANK, GPC-OPT succeed 2, 3, 4 respectively.

Fig. 10(b)(c) show the trajectories for both of these tests. More testing trajectories are shown in Appendix B and supplementary videos.

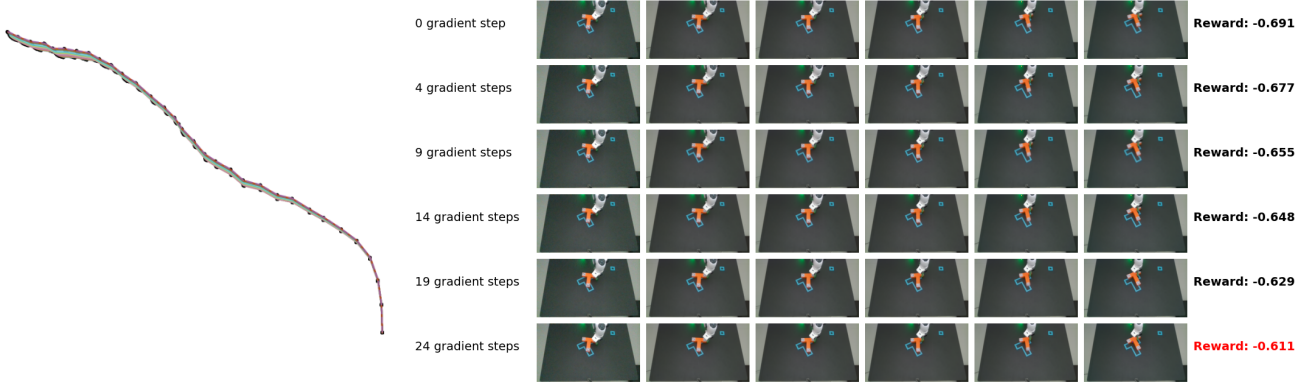
**Quality of world model predictions.** Fig. 7 and Fig. 8 show the quality of world model prediction for GPC-RANK and GPC-OPT, having collisions during push-T. The images shown are all **predicted** by the world model. With adding some collision objects, the world model is not only able to give near perfect prediction (i.e. no deformation) for a complex scene composing several objects, but also it can accurately predict the dynamics among these objects.

3) *Generalization to unseen cases*: Last but not least, we want to understand whether GPC can help when generalizing to unseen cases. We use the policy and world model trained with push-T, push-T colliding A, push-T colliding A&R expert demos. But we perform the test to push T when an object of letter “R” is on top of the target. This situation has never been seen in any of the training data. We test three different starting positions for T and R.

**Performance.** GPC-RANK and GPC-OPT succeed in all of the three tests while baseline model fails in one of the cases. The reason behind this is that when generalizing to unseen cases,



(a) World model prediction in GPC-RANK



(b) World model prediction in GPC-OPT

Fig. 6: WORLD MODEL PREDICTION IN GPC FOR PUSH-T. [Top] For GPC-RANK, we show the action proposals (left) and corresponding image predictions (right) from time  $t$  to  $t + T$ . Every row corresponds to the set of image consequences for an action proposal. We only pick 6 action proposals and downsample the image prediction sequences for displaying purpose. [Bottom] For GPC-OPT, we show optimized action proposals (left) and corresponding image predictions (right) from time  $t$  to  $t + T$ . Every row corresponds to the set of image consequences for an optimized action proposal at optimization step  $i$ . We only pick 6 optimization steps and downsample the image prediction sequences for displaying purpose.

the policy’s performance degrades. So we need to either generate more samples from the action policy’s distribution (like giving more opportunities to generate an optimal proposal) or do gradient ascent to optimize the action proposal.

Fig. 11 shows one test. More testing trajectories are shown in Appendix B and supplementary videos.

**Quality of world model predictions.** Fig. 9 shows the quality of world model prediction of push T under collision in unseen scenarios for GPC-RANK and GPC-OPT. A scenario only composes of T and R is never seen in the training data. However, our world model can still give good predictions for action sequences here. It verifies the ability of generalization for our world model.

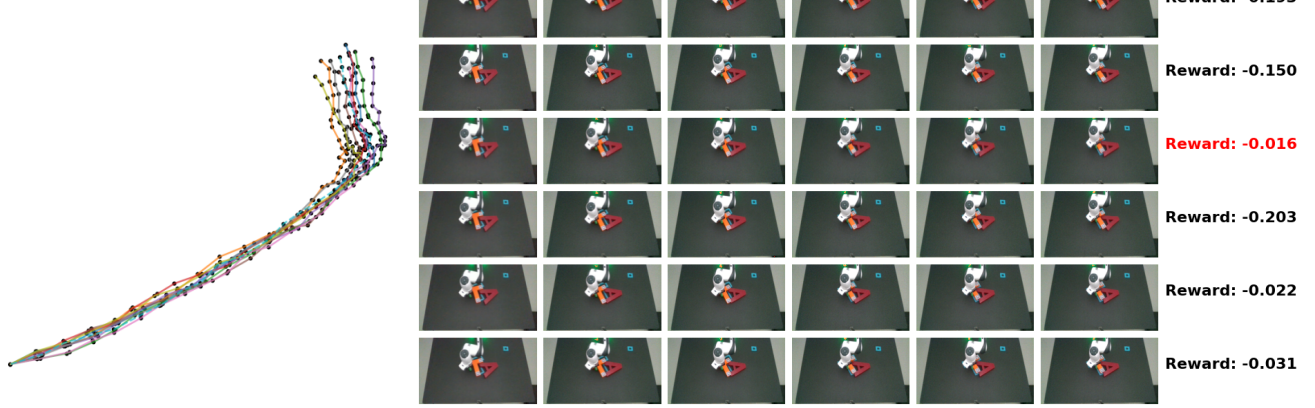
**Remark 3** (Hallucination). *One of the important issues of generative modeling is hallucination, and our visual world model is no exception. In particular, there are several cases where the world model predicts images of the future that violates rigid-body physics. For example, the objects T, A,*

*and R may penetrate each other, as we show in Appendix C. Interestingly, even though the predictions can violate physics, using such predictions for planning still leads to GPC’s superior performance. We believe learning a visual world model that strictly satisfies the laws of physics remains a challenging task, and strategies such as data scaling and baking in physics priors may help solve this challenge.*

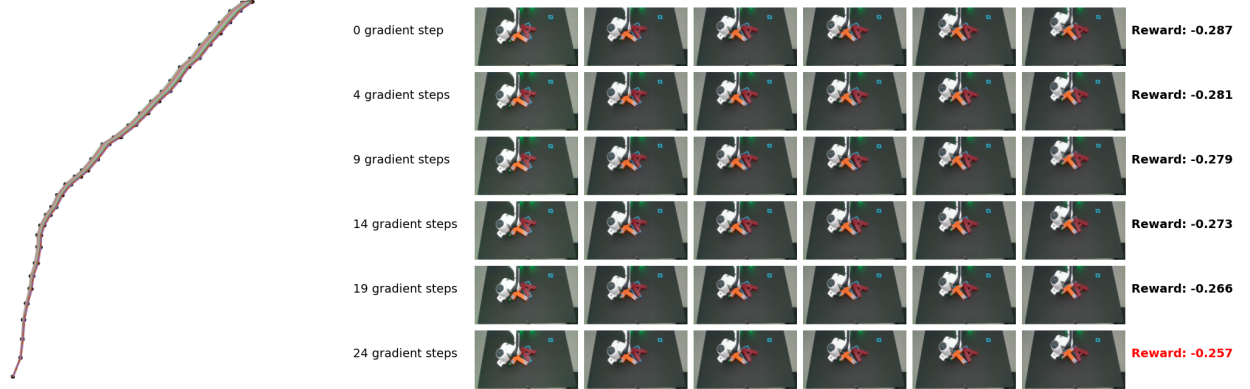
## V. RELATED WORK

**Generative modeling for robotics.** A large body of recent work has explored how generative models can be integrated with robotics [52]. Generative models have been used extensively to represent policies [43, 42, 27, 15, 11, 7, 36, 29], where models are often trained using large datasets of task demonstrations. In addition, generative models have also been used as a source of generating additional data [55, 54, 14] as well as models of the dynamics of the world [40, 12, 60].

Finally, a large body of work has explored how generative



(a) World model prediction in GPC-RANK



(b) World model prediction in GPC-OPT

Fig. 7: WORLD MODEL PREDICTION IN GPC FOR PUSH-T WITH COLLISION OF A. [Top] For GPC-RANK, we show the action proposals (left) and corresponding image predictions (right) from time  $t$  to  $t + T$ . Every row corresponds to the set of image consequences for an action proposal. We only pick 6 action proposals and downsample the image prediction sequences for displaying purpose. [Bottom] For GPC-OPT, we show optimized action proposals (left) and corresponding image predictions (right) from time  $t$  to  $t + T$ . Every row corresponds to the set of image consequences for an optimized action proposal at optimization step  $i$ . We only pick 6 optimization steps and downsample the image prediction sequences for displaying purpose.

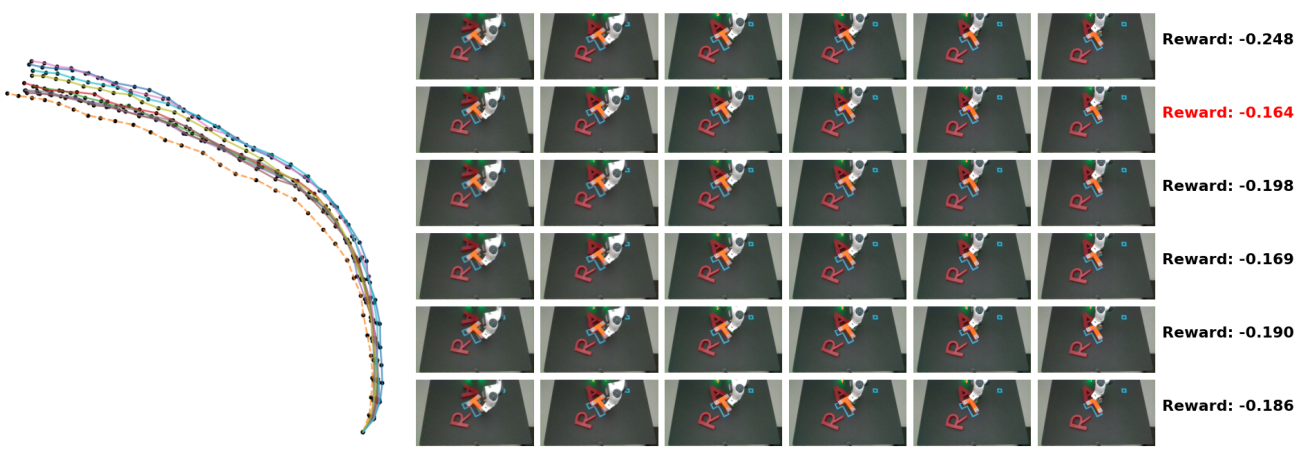
models can be used for planning [28, 3, 59, 13, 41]. Such methods directly train a generative model over sequences of state and action trajectories, and use the generation process to optimize actions. Different from these works, our work proposes a generative and predictive control (GPC) framework that combines a generative policy with a predictive world model through online planning to obtain more robust policy execution on new instances of a task. The modular design of GPC also allows for training foundation policies and foundation world models separately, using different data.

**Visual world modeling.** Learning predictive visual models of the world has a long history [58, 45, 22, 47]. Recently, video generative models have emerged as a powerful tool for modeling the physical world [19, 60, 39, 33, 53, 9, 8]. Such models have been used to initialize policies [19, 33, 9], as interactive simulators [60, 39, 8], and integrated with downstream planning [18, 53]. Different from these works, our

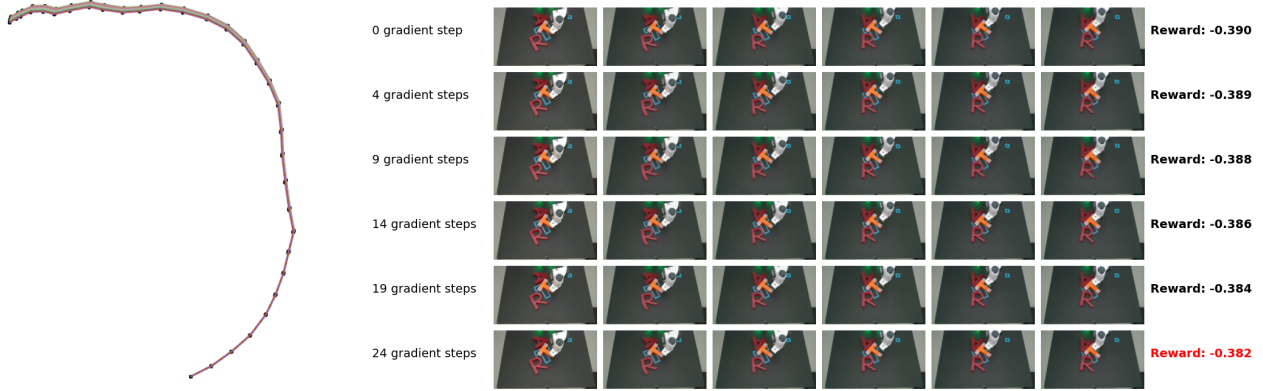
work uses a video model as an *action-conditioned dynamics model* that enables us to build a generative control framework that online computes a sequence of actions to optimizes a task-specific reward function.

## VI. CONCLUSION

We presented generative predictive control (GPC), a learning control paradigm that combines a generative policy with a predictive world model during online planning. It is worth noting that GPC bears great similarity with the classical literature on predictive control in the sense that the dynamics model is first identified and then optimization is performed online to decide actions. The new insights offered by GPC, perhaps, are that (a) modern conditional diffusion models provide a powerful tool to learn controllable action-conditioned visual world models; and (b) a generative policy trained from behavior cloning provides good warmstarts for online optimization



(a) World model prediction in GPC-RANK



(b) World model prediction in GPC-OPT

Fig. 8: WORLD MODEL PREDICTION IN GPC FOR PUSH-T WITH COLLISION OF A AND R. [Top] For GPC-RANK, we show the action proposals (left) and corresponding image predictions (right) from time  $t$  to  $t + T$ . Every row corresponds to the set of image consequences for an action proposal. We only pick 6 action proposals and downsample the image prediction sequences for displaying purpose. [Bottom] For GPC-OPT, we show optimized action proposals (left) and corresponding image predictions (right) from time  $t$  to  $t + T$ . Every row corresponds to the set of image consequences for an optimized action proposal at optimization step  $i$ . We only pick 6 optimization steps and downsample the image prediction sequences for displaying purpose.

that seem promising to partially tackle the nonconvexity of online optimization. Through an in-depth investigation on planar pushing—both simulated and real—we demonstrated the superior robustness of GPC in both state-based and vision-based robotic manipulation.

**Limitations.** Two issues are worth highlighting. The first issue is already mentioned in Remark 3 and concerns the problem of hallucinating future predictions that violate the laws of physics. To address this, it may be possible to leverage the so-called world foundation models [2]—trained on Internet-scale videos—and finetune them for specific robotic tasks. The second issue is associated with the computational complexity of using an expensive diffusion-based world model in online planning. It is worth noting that, although GPC dominates the baseline in terms of success rates, it is generally slower than the baseline due to predicting the future using the world model. A promising solution is to leverage consistency models [51]

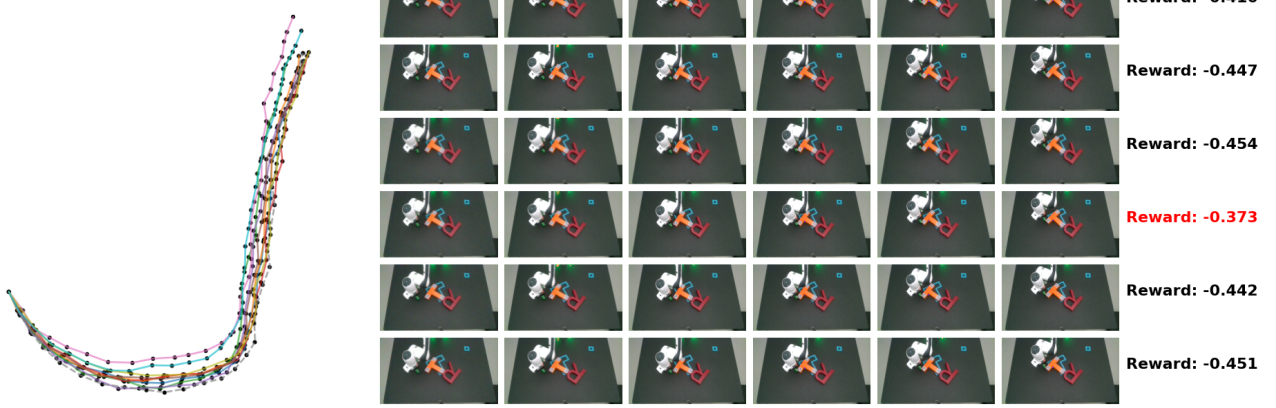
and one-step diffusion [61] for faster world model prediction.

#### ACKNOWLEDGMENTS

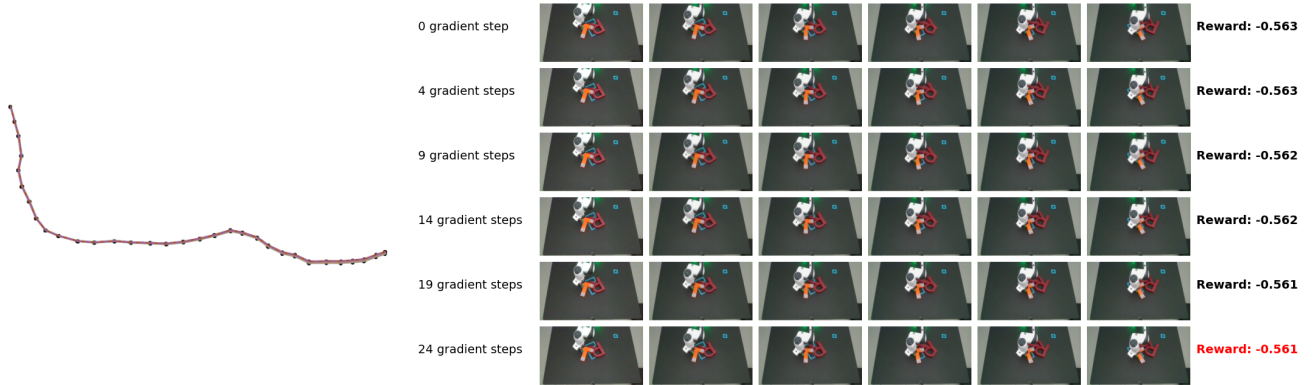
This work was partially supported by the Harvard University Dean’s Competitive Fund for Promising Scholarship. The authors thank William Zhang for his help on hardware design and prototyping. We thank members of the Harvard Computational Robotics Group for their contributions in collecting demonstrations. Their collective support has been instrumental in the completion of this work.

#### REFERENCES

- [1] Behcet Acikmese and Scott R. Ploen. Convex programming approach to powered descent guidance for mars landing. *Journal of Guidance, Control, and Dynamics*, 30(5):1353–1366, 2007. 1
- [2] Niket Agarwal, Arslan Ali, Maciej Bala, Yogesh Balaji, Erik Barker, Tiffany Cai, Prithvijit Chattopadhyay,



(a) World model prediction in GPC-RANK



(b) World model prediction in GPC-OPT

Fig. 9: WORLD MODEL PREDICTION IN GPC FOR PUSH-T WITH COLLISION OF R. [Top] For GPC-RANK, we show the action proposals (left) and corresponding image predictions (right) from time  $t$  to  $t + T$ . Every row corresponds to the set of image consequences for an action proposal. We only pick 6 action proposals and downsample the image prediction sequences for displaying purpose. [Bottom] For GPC-OPT, we show optimized action proposals (left) and corresponding image predictions (right) from time  $t$  to  $t + T$ . Every row corresponds to the set of image consequences for an optimized action proposal at optimization step  $i$ . We only pick 6 optimization steps and downsample the image prediction sequences for displaying purpose.

Yongxin Chen, Yin Cui, Yifan Ding, et al. Cosmos world foundation model platform for physical ai. *arXiv preprint arXiv:2501.03575*, 2025. 11

[3] Anurag Ajay, Yilun Du, Abhi Gupta, Joshua Tenenbaum, Tommi Jaakkola, and Pulkit Agrawal. Is conditional generative modeling all you need for decision-making? *arXiv preprint arXiv:2211.15657*, 2022. 10

[4] Ilge Akkaya, Marcin Andrychowicz, Maciek Chociej, Mateusz Litwin, Bob McGrew, Arthur Petron, Alex Paino, Matthias Plappert, Glenn Powell, Raphael Ribas, et al. Solving rubik’s cube with a robot hand. *arXiv preprint arXiv:1910.07113*, 2019. 1

[5] Eloi Alonso, Adam Jelley, Vincent Micheli, Anssi Kanervisto, Amos Storkey, Tim Pearce, and François Fleuret. Diffusion for world modeling: Visual details matter in atari. In *Thirty-eighth Conference on Neural Information Processing Systems*. 5

[6] Eloi Alonso, Adam Jelley, Vincent Micheli, Anssi Kan-

ervisto, Amos Storkey, Tim Pearce, and François Fleuret. Diffusion for world modeling: Visual details matter in atari. *arXiv preprint arXiv:2405.12399*, 2024. 2

[7] Lars Ankile, Anthony Simeonov, Idan Shenfeld, Marcel Torne, and Pulkit Agrawal. From imitation to refinement–residual rl for precise assembly. *arXiv preprint arXiv:2407.16677*, 2024. 2, 9

[8] Amir Bar, Gaoyue Zhou, Danny Tran, Trevor Darrell, and Yann LeCun. Navigation world models. *arXiv preprint arXiv:2412.03572*, 2024. 10

[9] Homanga Bharadhwaj, Debidatta Dwibedi, Abhinav Gupta, Shubham Tulsiani, Carl Doersch, Ted Xiao, Dhruv Shah, Fei Xia, Dorsa Sadigh, and Sean Kirmani. Gen2act: Human video generation in novel scenarios enables generalizable robot manipulation. *arXiv preprint arXiv:2409.16283*, 2024. 10

[10] Kevin Black, Mitsuhiro Nakamoto, Pranav Atreya, Homer Walke, Chelsea Finn, Aviral Kumar, and Sergey

Levine. Zero-shot robotic manipulation with pre-trained image-editing diffusion models. *arXiv preprint arXiv:2310.10639*, 2023. 2

[11] Anthony Brohan, Noah Brown, Justice Carbajal, Yevgen Chebotar, Xi Chen, Krzysztof Choromanski, Tianli Ding, Danny Driess, Avinava Dubey, Chelsea Finn, et al. RT-2: Vision-language-action models transfer web knowledge to robotic control. *arXiv preprint arXiv:2307.15818*, 2023. 9

[12] Arunkumar Byravan, Felix Leeb, Franziska Meier, and Dieter Fox. SE3-Pose-Nets: Structured deep dynamics models for visuomotor planning and control. *arXiv preprint arXiv:1710.00489*, 2017. 9

[13] Joao Carvalho, An T Le, Mark Baierl, Dorothea Koert, and Jan Peters. Motion planning diffusion: Learning and planning of robot motions with diffusion models. In *2023 IEEE/RSJ International Conference on Intelligent Robots and Systems (IROS)*, pages 1916–1923. IEEE, 2023. 10

[14] Zoey Chen, Sho Kiami, Abhishek Gupta, and Vikash Kumar. GenAug: Retargeting behaviors to unseen situations via generative augmentation. *arXiv preprint arXiv:2302.06671*, 2023. 9

[15] Cheng Chi, Zhenjia Xu, Siyuan Feng, Eric Cousineau, Yilun Du, Benjamin Burchfiel, Russ Tedrake, and Shuran Song. Diffusion policy: Visuomotor policy learning via action diffusion. *The International Journal of Robotics Research*, 2023. 2, 3, 5, 6, 7, 9

[16] Moritz Diehl and Sébastien Gros. Numerical optimal control. *Optimization in Engineering Center (OPTEC)*, 2011. 2, 3

[17] Zihan Ding, Amy Zhang, Yuandong Tian, and Qingjing Zheng. Diffusion world model: Future modeling beyond step-by-step rollout for offline reinforcement learning. *arXiv preprint arXiv:2402.03570*, 2024. 2

[18] Yilun Du, Mengjiao Yang, Pete Florence, Fei Xia, Ayaan Wahid, Brian Ichter, Pierre Sermanet, Tianhe Yu, Pieter Abbeel, Joshua B Tenenbaum, et al. Video language planning. *arXiv preprint arXiv:2310.10625*, 2023. 10

[19] Yilun Du, Sherry Yang, Bo Dai, Hanjun Dai, Ofir Nachum, Josh Tenenbaum, Dale Schuurmans, and Pieter Abbeel. Learning universal policies via text-guided video generation. *Advances in Neural Information Processing Systems*, 36, 2024. 2, 7, 10

[20] Chelsea Finn and Sergey Levine. Deep visual foresight for planning robot motion. In *2017 IEEE International Conference on Robotics and Automation (ICRA)*, pages 2786–2793. IEEE, 2017. 4, 7

[21] Roya Firoozi, Johnathan Tucker, Stephen Tian, Anirudha Majumdar, Jiankai Sun, Weiyu Liu, Yuke Zhu, Shuran Song, Ashish Kapoor, Karol Hausman, et al. Foundation models in robotics: Applications, challenges, and the future. *The International Journal of Robotics Research*, page 02783649241281508, 2023. 2

[22] David Ha and Jürgen Schmidhuber. World models. *arXiv preprint arXiv:1803.10122*, 2018. 2, 10

[23] Danijar Hafner, Timothy Lillicrap, Mohammad Norouzi, and Jimmy Ba. Mastering atari with discrete world models. *arXiv preprint arXiv:2010.02193*, 2020. 2

[24] Jonathan Ho, Ajay Jain, and Pieter Abbeel. Denoising diffusion probabilistic models. *Advances in neural information processing systems*, 33:6840–6851, 2020. 3

[25] Jonathan Ho, Tim Salimans, Alexey Gritsenko, William Chan, Mohammad Norouzi, and David J Fleet. Video diffusion models. *Advances in Neural Information Processing Systems*, 35:8633–8646, 2022. 2

[26] François Robert Hogan and Alberto Rodriguez. Feedback control of the pusher-slider system: A story of hybrid and underactuated contact dynamics. In *Algorithmic Foundations of Robotics XII: Proceedings of the Twelfth Workshop on the Algorithmic Foundations of Robotics*, pages 800–815. Springer, 2020. 4

[27] Eric Jang, Alex Irpan, Mohi Khansari, Daniel Kappler, Frederik Ebert, Corey Lynch, Sergey Levine, and Chelsea Finn. BC-Z: Zero-shot task generalization with robotic imitation learning. In *Conference on Robot Learning*, pages 991–1002. PMLR, 2022. 9

[28] Michael Janner, Yilun Du, Joshua B Tenenbaum, and Sergey Levine. Planning with diffusion for flexible behavior synthesis. *arXiv preprint arXiv:2205.09991*, 2022. 2, 10

[29] Yunfan Jiang, Agrim Gupta, Zichen Zhang, Guanzhi Wang, Yongqiang Dou, Yanjun Chen, Li Fei-Fei, Anima Anandkumar, Yuke Zhu, and Linxi Fan. VIMA: General robot manipulation with multimodal prompts. *arXiv preprint arXiv:2210.03094*, 2(3):6, 2022. 9

[30] Shucheng Kang, Xiaoyang Xu, Jay Sarva, Ling Liang, and Heng Yang. Fast and certifiable trajectory optimization. *International Workshop on the Algorithmic Foundations of Robotics (WAFR)*, 2024. 1

[31] Elia Kaufmann, Antonio Loquercio, René Ramftl, Matthias Müller, Vladlen Koltun, and Davide Scaramuzza. Deep drone acrobatics. *arXiv preprint arXiv:2006.05768*, 2020. 1

[32] Moo Jin Kim, Karl Pertsch, Siddharth Karamcheti, Ted Xiao, Ashwin Balakrishna, Suraj Nair, Rafael Rafailov, Ethan Foster, Grace Lam, Pannag Sanketi, et al. Open-VLA: An open-source vision-language-action model. *arXiv preprint arXiv:2406.09246*, 2024. 2

[33] Po-Chen Ko, Jiayuan Mao, Yilun Du, Shao-Hua Sun, and Joshua B Tenenbaum. Learning to act from actionless videos through dense correspondences. *arXiv preprint arXiv:2310.08576*, 2023. 10

[34] Ilya Kostrikov, Ashvin Nair, and Sergey Levine. Offline reinforcement learning with implicit q-learning. *arXiv preprint arXiv:2110.06169*, 2021. 18

[35] Quentin Le Lidec, Wilson Jallet, Louis Montaut, Ivan Laptev, Cordelia Schmid, and Justin Carpentier. Contact models in robotics: a comparative analysis. *IEEE Transactions on Robotics*, 2024. 2

[36] Seungjae Lee, Yibin Wang, Haritheja Etukuru, H Jin Kim, Nur Muhammad Mahi Shafiullah, and Lerrel Pinto.

Behavior generation with latent actions. *arXiv preprint arXiv:2403.03181*, 2024. 9

[37] Ljung Lennart. System identification: theory for the user. *PTR Prentice Hall, Upper Saddle River, NJ*, 28: 540, 1999. 3

[38] Xuanlin Li, Kyle Hsu, Jiayuan Gu, Karl Pertsch, Oier Mees, Homer Rich Walke, Chuyuan Fu, Ishikaa Lunawat, Isabel Sieh, Sean Kirmani, et al. Evaluating real-world robot manipulation policies in simulation. *arXiv preprint arXiv:2405.05941*, 2024. 2

[39] Junbang Liang, Ruoshi Liu, Ege Ozguroglu, Sruthi Sudhakar, Achal Dave, Pavel Tokmakov, Shuran Song, and Carl Vondrick. Dreamitate: Real-world visuomotor policy learning via video generation. *arXiv preprint arXiv:2406.16862*, 2024. 10

[40] Weiyu Liu, Tucker Hermans, Sonia Chernova, and Chris Paxton. Structdiffusion: Object-centric diffusion for semantic rearrangement of novel objects. In *Workshop on Language and Robotics at CoRL 2022*, 2022. 9

[41] Yunhao Luo, Chen Sun, Joshua B. Tenenbaum, and Yilun Du. Potential based diffusion motion planning. In *Forty-first International Conference on Machine Learning*, 2024. 10

[42] Corey Lynch, Mohi Khansari, Ted Xiao, Vikash Kumar, Jonathan Tompson, Sergey Levine, and Pierre Sermanet. Learning latent plans from play. In *Conference on robot learning*, pages 1113–1132. PMLR, 2020. 9

[43] Ajay Mandlekar, Fabio Ramos, Byron Boots, Silvio Savarese, Li Fei-Fei, Animesh Garg, and Dieter Fox. IRIS: Implicit reinforcement without interaction at scale for learning control from offline robot manipulation data. In *2020 IEEE International Conference on Robotics and Automation (ICRA)*, pages 4414–4420. IEEE, 2020. 9

[44] Mitsuhiro Nakamoto, Oier Mees, Aviral Kumar, and Sergey Levine. Steering your generalists: Improving robotic foundation models via value guidance. *arXiv preprint arXiv:2410.13816*, 2024. 2, 6, 18

[45] Junhyuk Oh, Xiaoxiao Guo, Honglak Lee, Richard L Lewis, and Satinder Singh. Action-conditional video prediction using deep networks in atari games. *Advances in neural information processing systems*, 28, 2015. 10

[46] Edwin Olson. AprilTag: A robust and flexible visual fiducial system. In *2011 IEEE international conference on robotics and automation*, pages 3400–3407. IEEE, 2011. 4, 7, 8

[47] Sergiu Oprea, Pablo Martinez-Gonzalez, Alberto Garcia-Garcia, John Alejandro Castro-Vargas, Sergio Orts-Escolano, Jose Garcia-Rodriguez, and Antonis Argyros. A review on deep learning techniques for video prediction. *IEEE Transactions on Pattern Analysis and Machine Intelligence*, 44(6):2806–2826, 2020. 10

[48] Han Qi, Haocheng Yin, and Heng Yang. Control-oriented clustering of visual latent representation. *arXiv preprint arXiv:2410.05063*, 2024. 2

[49] Nikita Rudin, David Hoeller, Philipp Reist, and Marco Hutter. Learning to walk in minutes using massively parallel deep reinforcement learning. In *Conference on Robot Learning*, pages 91–100. PMLR, 2022. 1

[50] Elad Sharony, Heng Yang, Tong Che, Marco Pavone, Shie Mannor, and Peter Karkus. Learning multiple initial solutions to optimization problems. *arXiv preprint arXiv:2411.02158*, 2024. 3

[51] Yang Song, Prafulla Dhariwal, Mark Chen, and Ilya Sutskever. Consistency models. *arXiv preprint arXiv:2303.01469*, 2023. 11

[52] Julen Urain, Ajay Mandlekar, Yilun Du, Mahi Shafullah, Danfei Xu, Katerina Fragkiadaki, Georgia Chalvatzaki, and Jan Peters. Deep generative models in robotics: A survey on learning from multimodal demonstrations. *arXiv preprint arXiv:2408.04380*, 2024. 2, 9

[53] Boyang Wang, Nikhil Sridhar, Chao Feng, Mark Van der Merwe, Adam Fishman, Nima Fazeli, and Jeong Joon Park. This&that: Language-gesture controlled video generation for robot planning. *arXiv preprint arXiv:2407.05530*, 2024. 10

[54] Lirui Wang, Yiyang Ling, Zhecheng Yuan, Mohit Shridhar, Chen Bao, Yuzhe Qin, Bailin Wang, Huazhe Xu, and Xiaolong Wang. GenSim: Generating robotic simulation tasks via large language models. *arXiv preprint arXiv:2310.01361*, 2023. 9

[55] Yufei Wang, Zhou Xian, Feng Chen, Tsun-Hsuan Wang, Yian Wang, Katerina Fragkiadaki, Zackory Erickson, David Held, and Chuang Gan. RoboGen: Towards unleashing infinite data for automated robot learning via generative simulation. *arXiv preprint arXiv:2311.01455*, 2023. 9

[56] Zhendong Wang, Jonathan J Hunt, and Mingyuan Zhou. Diffusion policies as an expressive policy class for offline reinforcement learning. *arXiv preprint arXiv:2208.06193*, 2022. 2

[57] Patrick M. Wensing, Michael Posa, Yue Hu, Adrien Escande, Nicolas Mansard, and Andrea Del Prete. Optimization-based control for dynamic legged robots. *IEEE Transactions on Robotics*, 2023. 1

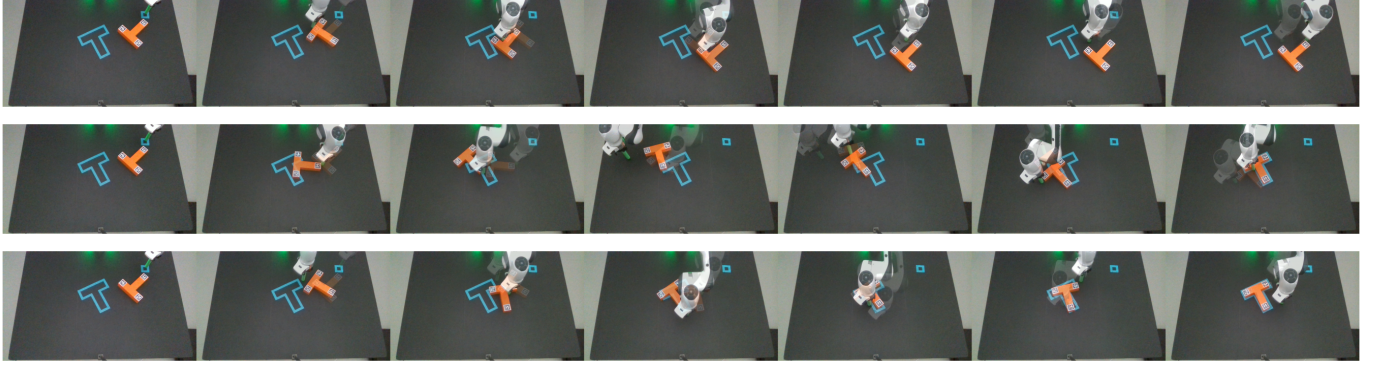
[58] Tianfan Xue, Jiajun Wu, Katherine Bouman, and Bill Freeman. Visual dynamics: Probabilistic future frame synthesis via cross convolutional networks. *Advances in neural information processing systems*, 29, 2016. 10

[59] Brian Yang, Huangyuan Su, Nikolaos Gkanatsios, Tsung-Wei Ke, Ayush Jain, Jeff Schneider, and Katerina Fragkiadaki. Diffusion-es: Gradient-free planning with diffusion for autonomous driving and zero-shot instruction following. *arXiv preprint arXiv:2402.06559*, 2024. 10

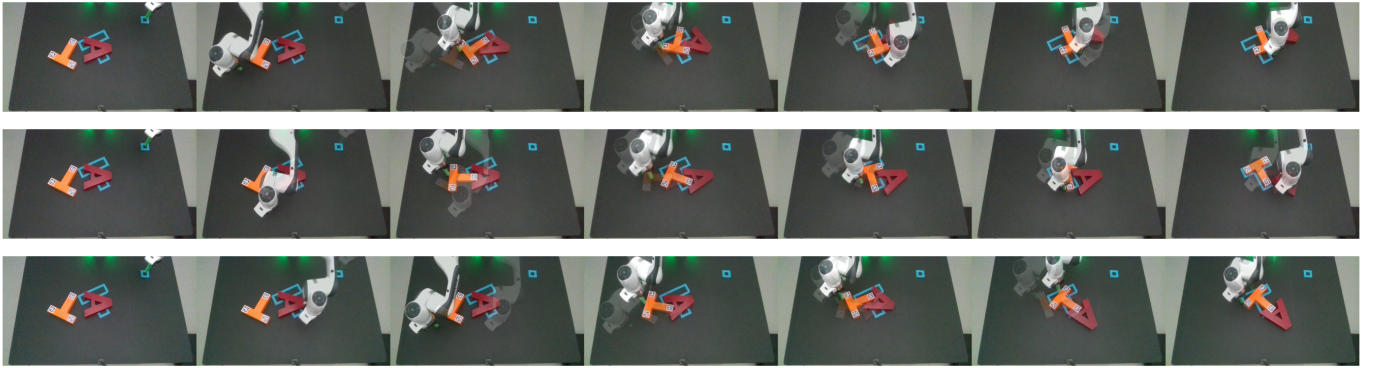
[60] Mengjiao Yang, Yilun Du, Kamyar Ghasemipour, Jonathan Tompson, Dale Schuurmans, and Pieter Abbeel. Learning interactive real-world simulators. *arXiv preprint arXiv:2310.06114*, 2023. 9, 10

[61] Tianwei Yin, Michaël Gharbi, Richard Zhang, Eli Shechtman, Fredo Durand, William T Freeman, and Tae-sung Park. One-step diffusion with distribution matching distillation. In *Proceedings of the IEEE/CVF Conference on Computer Vision and Pattern Recognition*, pages

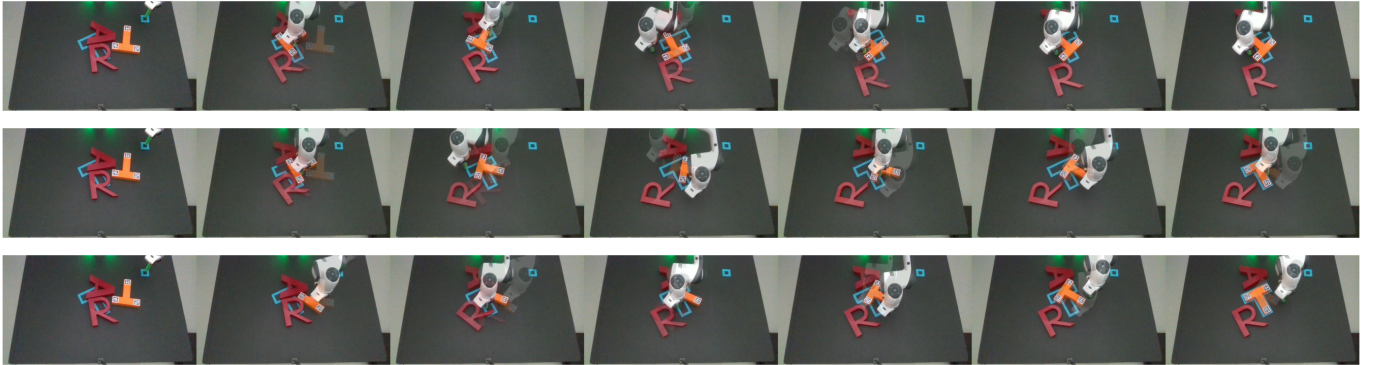
- [62] Alan Yu, Ge Yang, Ran Choi, Y Ravan, J Leonard, and P Isola. Learning agile visual locomotion from generated images. In *8th Annual Conference on Robot Learning*, 2024. 2
- [63] Tony Z Zhao, Jonathan Tompson, Danny Driess, Pete Florence, Kamyar Ghasemipour, Chelsea Finn, and Ayzaan Wahid. ALOHA Unleashed: A simple recipe for robot dexterity. *arXiv preprint arXiv:2410.13126*, 2024. 2
- [64] Yi Zhou, Connelly Barnes, Jingwan Lu, Jimei Yang, and Hao Li. On the continuity of rotation representations in neural networks. In *Proceedings of the IEEE/CVF conference on computer vision and pattern recognition*, pages 5745–5753, 2019. 4
- [65] Jihong Zhu, Andrea Cherubini, Claire Dune, David Navarro-Alarcon, Farshid Alambeigi, Dmitry Berenson, Fanny Ficuciello, Kensuke Harada, Jens Kober, Xiang Li, et al. Challenges and outlook in robotic manipulation of deformable objects. *IEEE Robotics & Automation Magazine*, 29(3):67–77, 2022. 2



(a) Test for push-T



(b) Test for push-T with collision of A



(c) Test for push-T with collision of A and R

Fig. 10: REAL-WORLD TESTS FOR PLAIN PUSH-T AND PUSH-T WITH COLLISION. In every test, top row shows trajectories of baseline model ( $K = 1, M = 0$ ), middle row shows trajectories of GPC-RANK ( $K = 10, M = 0$ ), and last row shows trajectories of GPC-OPT ( $K = 0, M = 25$ ). The first and last column show the initial and final position of the object, respectively. The middle five columns show overlaid trajectories generated by the policies. Results for other real-world tests are shown in Appendix B and supplementary videos.

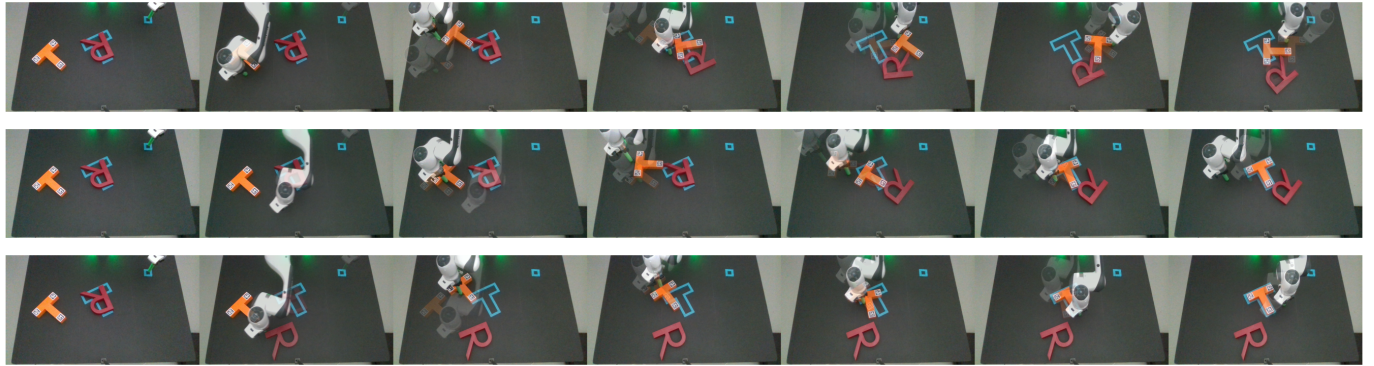


Fig. 11: REAL-WORLD TEST FOR OUT-OF-DOMAIN SCENE. In every test, top row shows trajectories of baseline model ( $K = 1, M = 0$ ), middle row shows trajectories of GPC-RANK ( $K = 10, M = 0$ ), and last row shows trajectories of GPC-OPT ( $K = 0, M = 25$ ). This displays GPC would help to make policy succeed in unseen scene while baseline failed. Remaining results for push-T with collision of R are shown in Appendix B and supplementary videos.

## APPENDIX

### A. Offline RL

While we rely on the world model to rank the action proposals, offline reinforcement learning ranks the action proposals using the value function [44]. It firstly learns the value function via offline RL pre-training, and then performs test-time action re-ranking via the learned value function. To train a value function  $Q(I_t, a_{t:t+T})$  where  $I_t$  is the state and  $a_{t:t+T}$  is the action chunk, we need to obtain a reward function that can be used to supervise the value function training. Consistent with the GPC-RANK method, we use registration error between the object and the target at  $I_{t+T+1}$  as the reward. We use the same length of action chunk ( $T$ ) as GPC-RANK for a fair comparison.

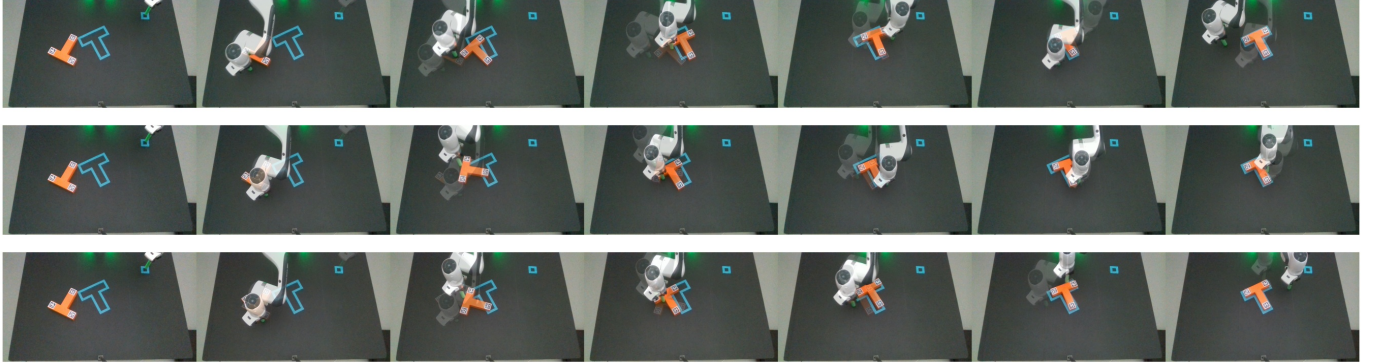
Implicit Q-learning (IQL) [34] is used as the offline RL method to pretrain a value function  $Q(I_t, a_{t:t+T})$ . For vision-based tasks, we use the pretrained vision encoder (ResNet18) from the action policy to encode the observation images  $I_t$  to latent vectors  $s_t$ . We then train the value function  $Q(s_t, a_{t:t+T})$ . With the trained value function, we can rank and select the action proposal with the highest Q-value.

$$a_{t:t+T}^{(k*)} = \arg \max_{a_{t:t+T}^{(k)}, k=1 \dots K} Q(s_t, a_{t:t+T}^{(k)}), \quad (A1)$$

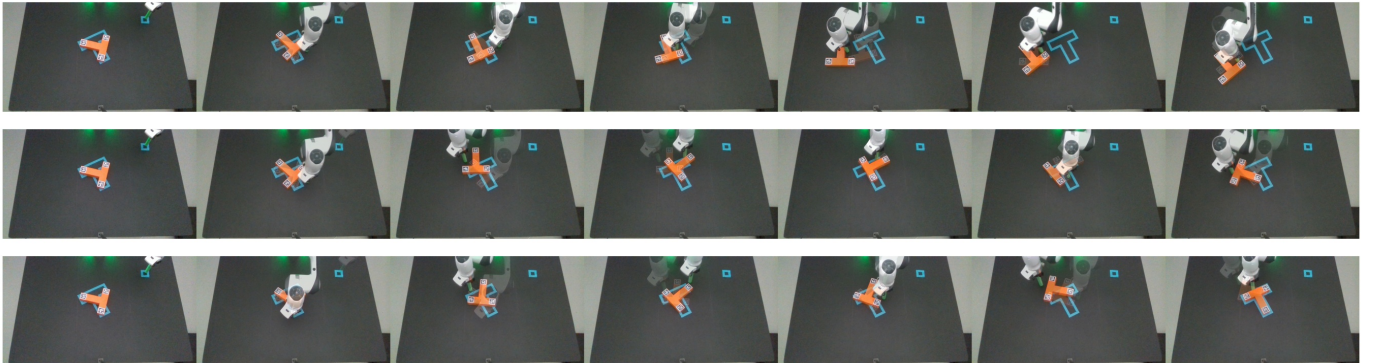
which is the same as the GPC-RANK method in (2).

## B. Real-World Experimental Results

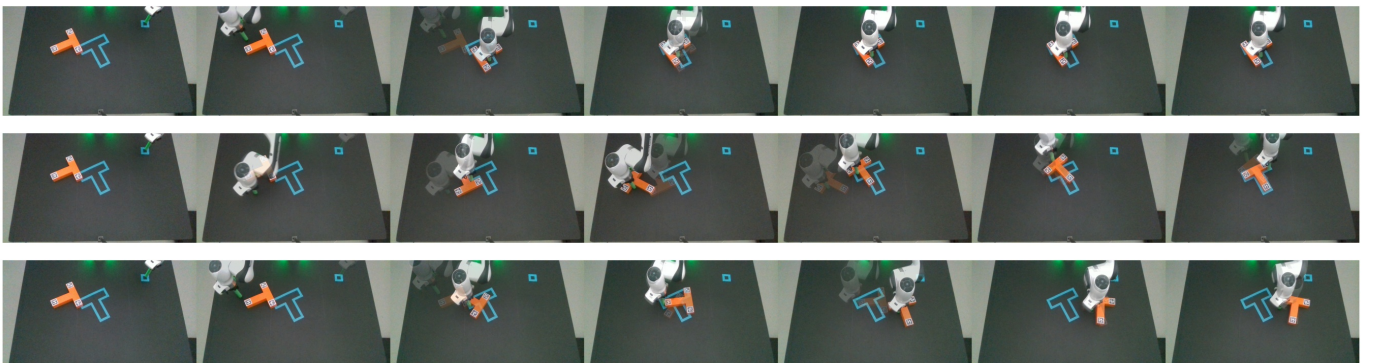
Here we provide more results for real-world experiments.



(a) Test 0 on Push-T



(b) Test 1 on Push-T

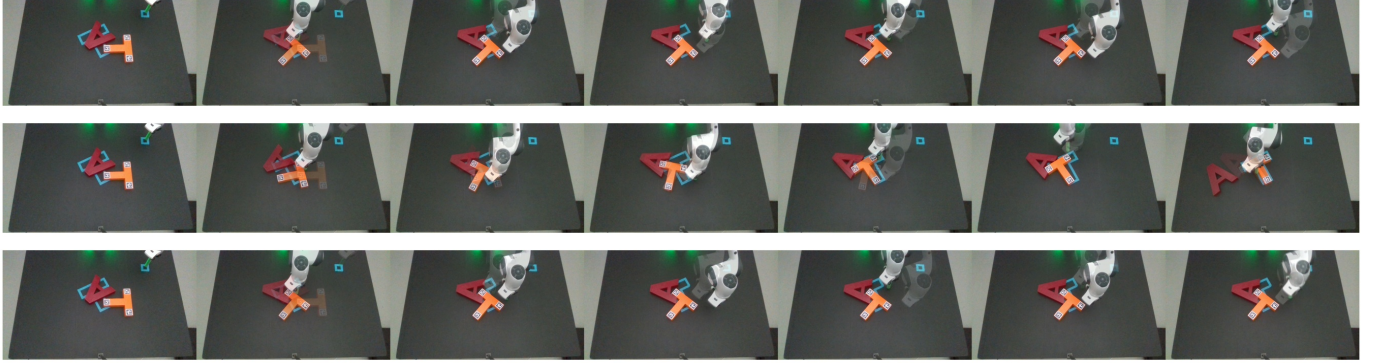


(c) Test 2 on Push-T

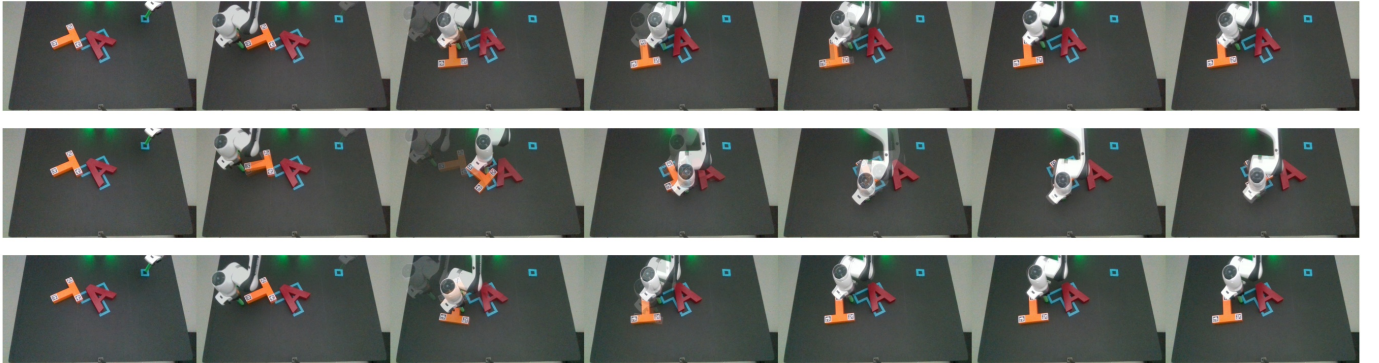
Fig. A1: MORE TRAJECTORY PLOTS FOR REAL-WORLD PUSH T. In every test, top row shows trajectories of baseline model ( $K = 1, M = 0$ ), middle row shows trajectories of GPC-RANK ( $K = 10, M = 0$ ), and last row shows trajectories of GPC-OPT ( $K = 0, M = 25$ ). The first and last column show the initial and final position of the object, respectively. The middle five columns show overlaid trajectories generated by the policies.

## C. Hallucination

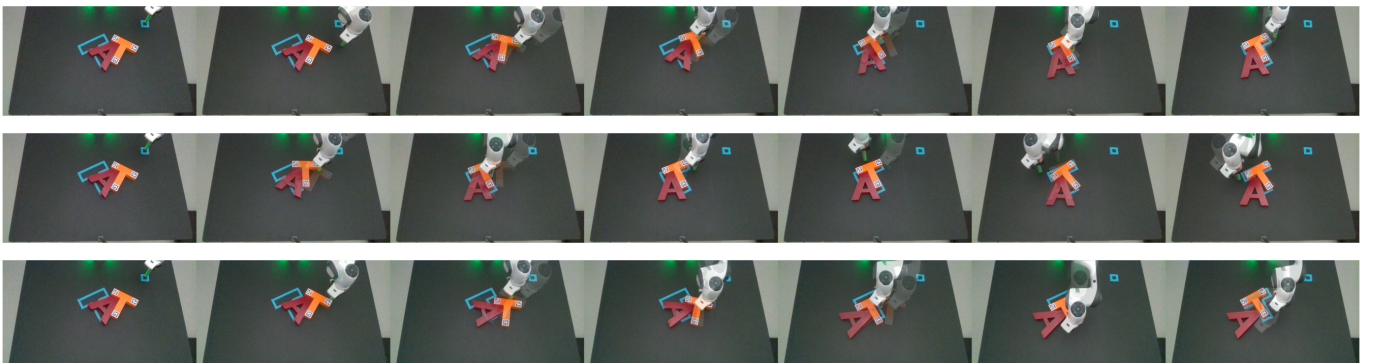
We show several visual world model predictions that are not physics-accurate.



(a) Test 0 on Push-T with collision of A

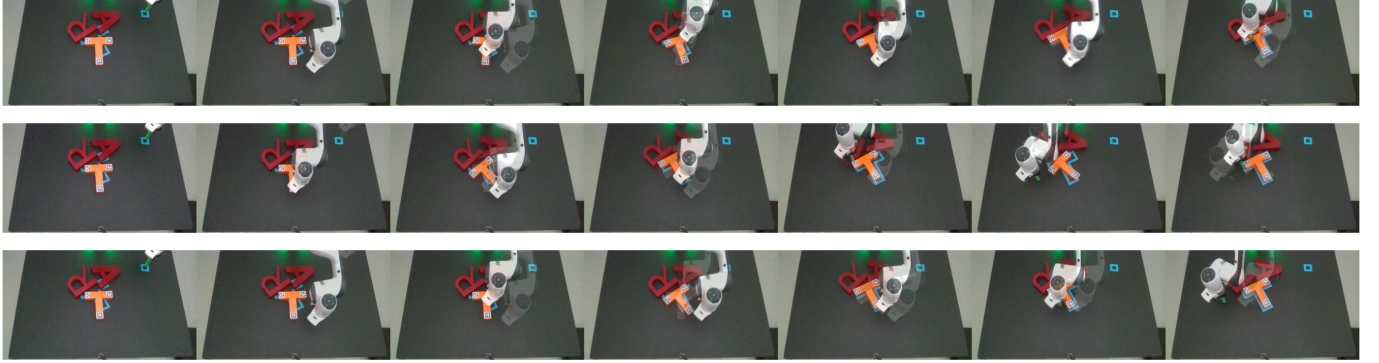


(b) Test 1 on Push-T with collision of A

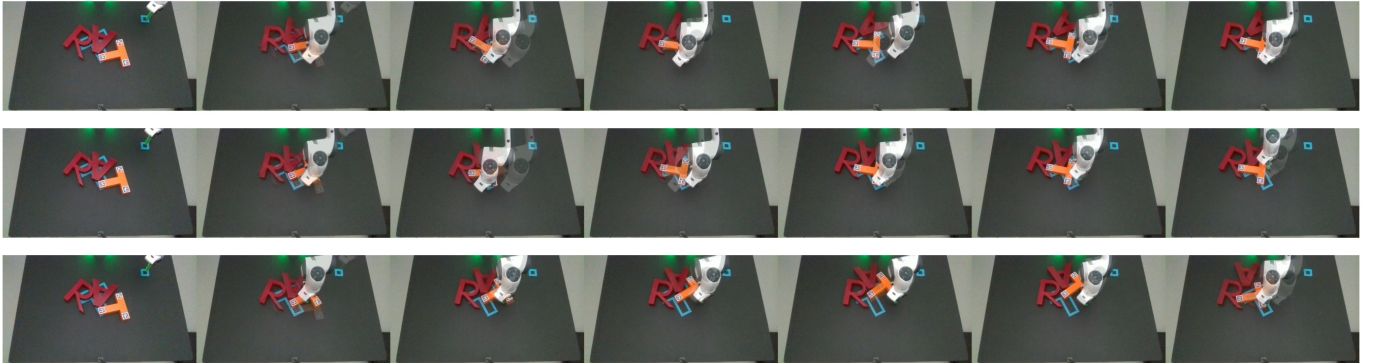


(c) Test 2 on Push-T with collision of A

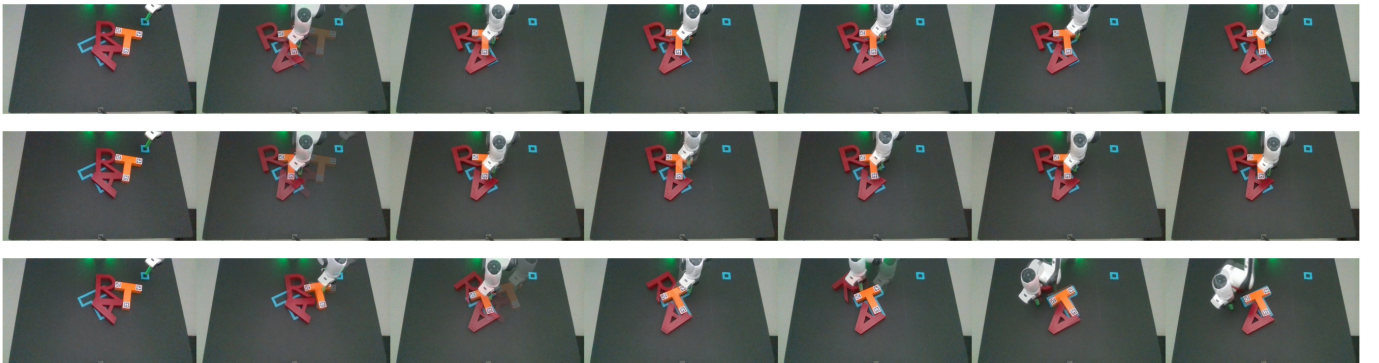
Fig. A2: MORE TRAJECTORY PLOTS FOR REAL-WORLD PUSH T WITH COLLISION OF A. In every test, top row shows trajectories of baseline model ( $K = 1, M = 0$ ), middle row shows trajectories of GPC-RANK ( $K = 10, M = 0$ ), and last row shows trajectories of GPC-OPT ( $K = 0, M = 25$ ). The first and last column show the initial and final position of the object, respectively. The middle five columns show overlaid trajectories generated by the policies.



(a) Test 0 on Push-T with collision of A and R

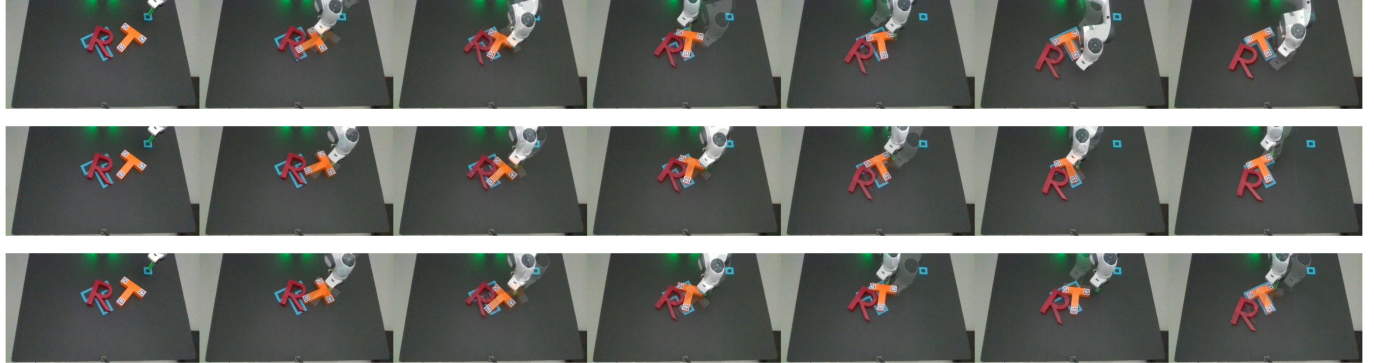


(b) Test 1 on Push-T with collision of A and R

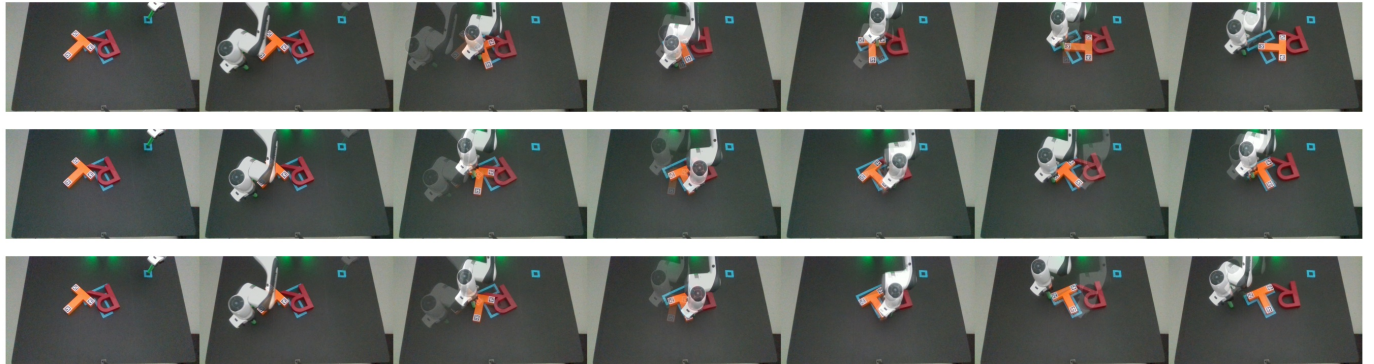


(c) Test 2 on Push-T with collision of A and R

Fig. A3: MORE TRAJECTORY PLOTS FOR REAL-WORLD PUSH T WITH COLLISION OF A AND R. In every test, top row shows trajectories of baseline model ( $K = 1, M = 0$ ), middle row shows trajectories of GPC-RANK ( $K = 10, M = 0$ ), and last row shows trajectories of GPC-OPT ( $K = 0, M = 25$ ). The first and last column show the initial and final position of the object, respectively. The middle five columns show overlaid trajectories generated by the policies.

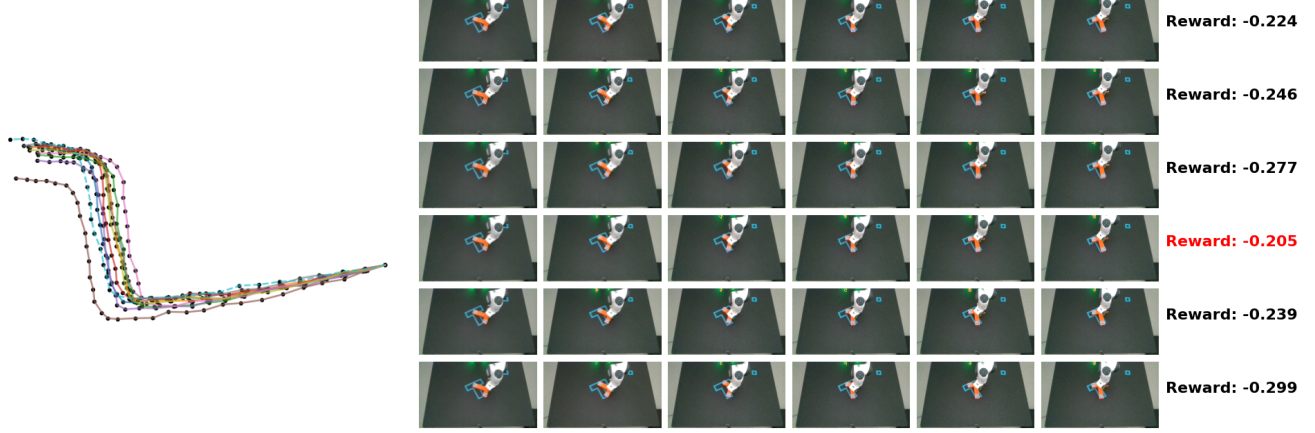


(a) Test 0 on Push-T with collision of R

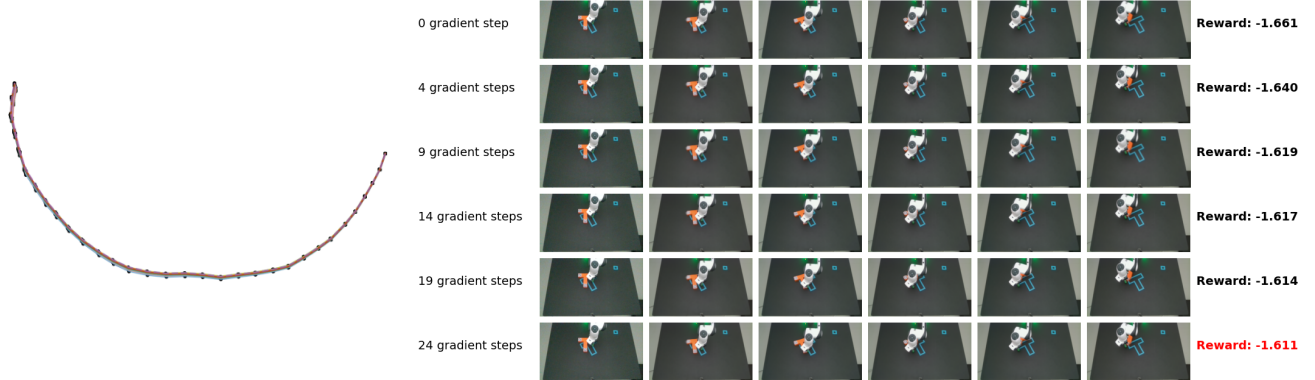


(b) Test 1 on Push-T with collision of R

Fig. A4: MORE TRAJECTORY PLOTS FOR REAL-WORLD PUSH T WITH COLLISION OF R (OUT-OF-DOMAIN SCENE). In every test, top row shows trajectories of baseline model ( $K = 1, M = 0$ ), middle row shows trajectories of GPC-RANK ( $K = 10, M = 0$ ), and last row shows trajectories of GPC-OPT ( $K = 0, M = 25$ ). The first and last column show the initial and final position of the object, respectively. The middle five columns show overlaid trajectories generated by the policies.

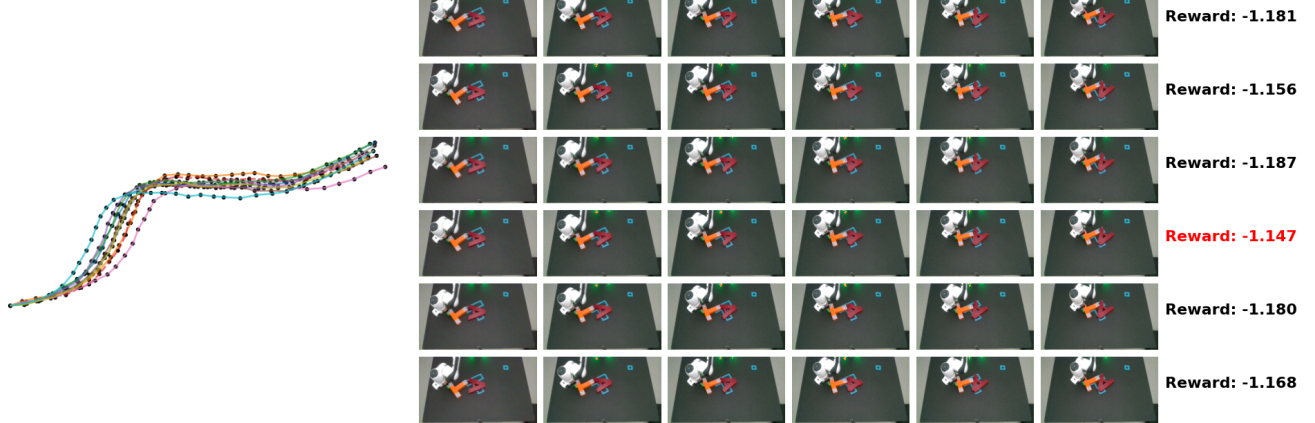


(a) World model prediction in GPC-RANK

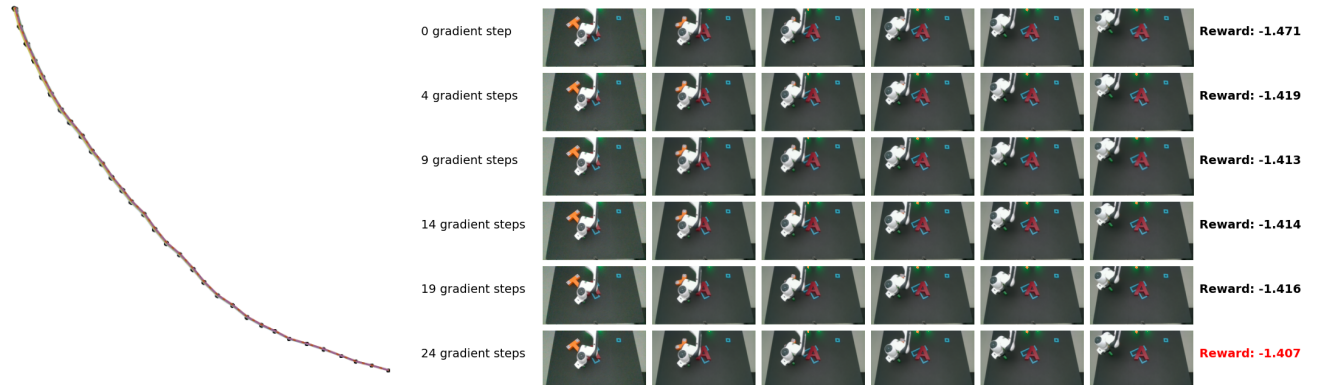


(b) World model prediction in GPC-OPT

Fig. A5: WORLD MODEL PREDICTION IN GPC FOR PUSH-T. [Top] For GPC-RANK, we show the action proposals (left) and corresponding image predictions (right) from time  $t$  to  $t + T$ . Every row corresponds to the set of image consequences for an action proposal. We only pick 6 action proposals and downsample the image prediction sequences for displaying purpose. [Bottom] For GPC-OPT, we show optimized action proposals (left) and corresponding image predictions (right) from time  $t$  to  $t + T$ . Every row corresponds to the set of image consequences for an optimized action proposal at optimization step  $i$ . We only pick 6 optimization steps and downsample the image prediction sequences for displaying purpose.

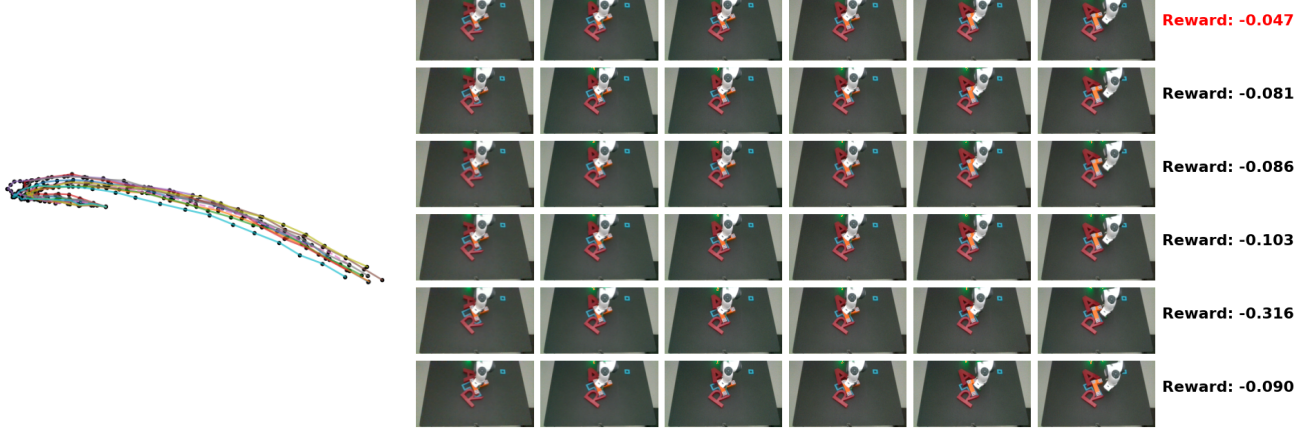


(a) World model prediction in GPC-RANK

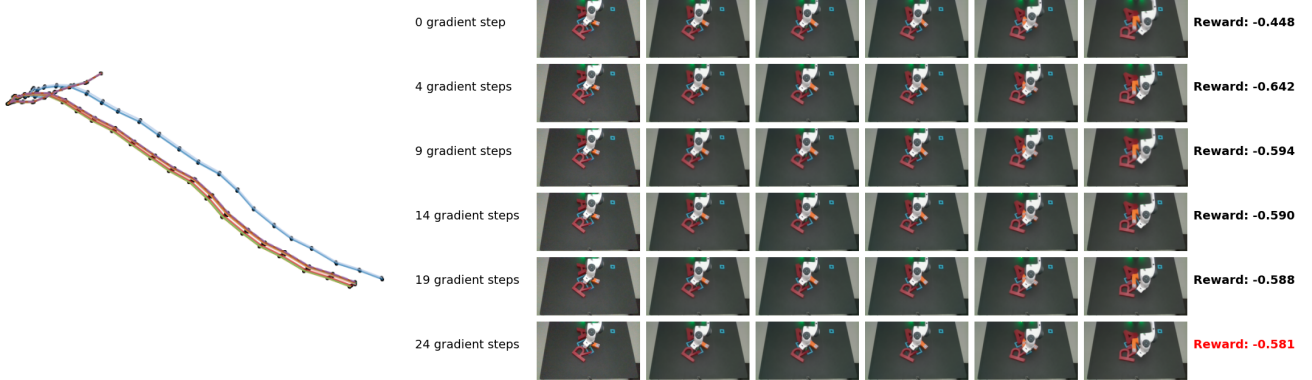


(b) World model prediction in GPC-OPT

Fig. A6: WORLD MODEL PREDICTION IN GPC FOR PUSH-T WITH COLLISION OF A. [Top] For GPC-RANK, we show the action proposals (left) and corresponding image predictions (right) from time  $t$  to  $t + T$ . Every row corresponds to the set of image consequences for an action proposal. We only pick 6 action proposals and downsample the image prediction sequences for displaying purpose. [Bottom] For GPC-OPT, we show optimized action proposals (left) and corresponding image predictions (right) from time  $t$  to  $t + T$ . Every row corresponds to the set of image consequences for an optimized action proposal at optimization step  $i$ . We only pick 6 optimization steps and downsample the image prediction sequences for displaying purpose.

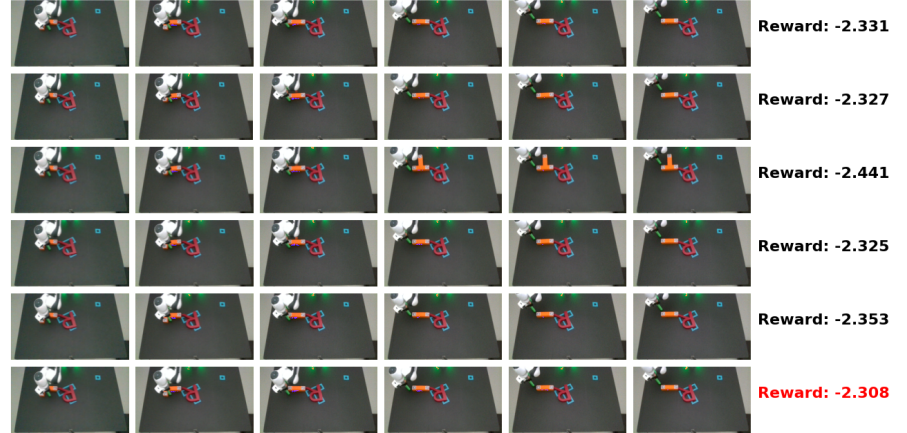
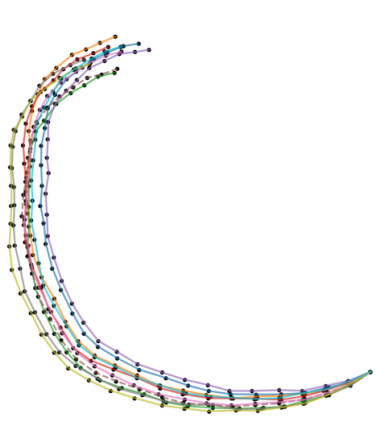


(a) World model prediction in GPC-RANK

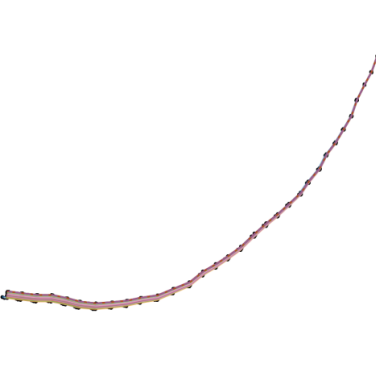


(b) World model prediction in GPC-OPT

Fig. A7: WORLD MODEL PREDICTION IN GPC FOR PUSH-T WITH COLLISION OF A AND R. [Top] For GPC-RANK, we show the action proposals (left) and corresponding image predictions (right) from time  $t$  to  $t + T$ . Every row corresponds to the set of image consequences for an action proposal. We only pick 6 action proposals and downsample the image prediction sequences for displaying purpose. [Bottom] For GPC-OPT, we show optimized action proposals (left) and corresponding image predictions (right) from time  $t$  to  $t + T$ . Every row corresponds to the set of image consequences for an optimized action proposal at optimization step  $i$ . We only pick 6 optimization steps and downsample the image prediction sequences for displaying purpose.



(a) World model prediction in GPC-RANK



(b) World model prediction in GPC-OPT

Fig. A8: WORLD MODEL PREDICTION IN GPC FOR PUSH-T WITH COLLISION OF R. [Top] For GPC-RANK, we show the action proposals (left) and corresponding image predictions (right) from time  $t$  to  $t + T$ . Every row corresponds to the set of image consequences for an action proposal. We only pick 6 action proposals and downsample the image prediction sequences for displaying purpose. [Bottom] For GPC-OPT, we show optimized action proposals (left) and corresponding image predictions (right) from time  $t$  to  $t + T$ . Every row corresponds to the set of image consequences for an optimized action proposal at optimization step  $i$ . We only pick 6 optimization steps and downsample the image prediction sequences for displaying purpose.